LA-UR- 01-5770

Title: Nuclear Effects in the Drell-Yan Process at RHIC and LHC

Author(s): B. Z. Kopeliovich, J. Raufeisen, A. V. Tarasov, and M. B. Johnson

Submitted to: *Physical Review C*
October 2001

Los Alamos
NATIONAL LABORATORY

Nuclear effects in the Drell-Yan process at RHIC and LHC

B.Z. Kopeliovich[a,b,c], J. Raufeisen[d], A.V. Tarasov[a,b,c], and M.B. Johnson[d]

[a] *Max-Planck Institut für Kernphysik, Postfach 103980, 69029 Heidelberg, Germany*
[b] *Institut für Theoretische Physik der Universität, 93040 Regensburg, Germany*
[c] *Joint Institute for Nuclear Research, Dubna, 141980 Moscow Region, Russia*
[d] *Los Alamos National Laboratory, MS H846, Los Alamos, NM 87545, USA*

Abstract

We study Drell-Yan (DY) dilepton production in proton(deuterium)-nucleus and in nucleus-nucleus collisions within the light-cone color dipole formalism. This approach is especially suitable for predicting nuclear effects in the DY cross section for heavy ion collisions, as it provides the impact parameter dependence of nuclear shadowing, a quantity that is not available from the standard parton model. For $p(D)+A$ collisions we calculate nuclear shadowing and investigate nuclear modification of the DY transverse momentum distribution at RHIC and LHC for kinematics corresponding to coherence length much longer than the nuclear size. Calculations are performed separately for transversely and longitudinally polarized DY photons and we make predictions for the dilepton angular distribution. Furthermore, we calculate nuclear broadening of the mean transverse momentum squared of DY dileptons as function of the nuclear mass number and energy. We also predict nuclear effects for the cross section of the DY process in heavy ion collisions. We found a substantial nuclear shadowing for valence quarks, stronger than for the sea.

1 Introduction

The cross section for the Drell-Yan (DY) process at the energies of the SPS suggests rather weak nuclear effects, if any at all (although measurements at small Feynman x_F are the only data available). However, the fixed target experiment E772 at Fermilab at 800 GeV [1] shows a sizeable nuclear suppression at large x_F. Although this suppression results from a complicated interplay between energy loss and shadowing [2, 3], shadowing effects are expected to be much stronger and span the entire range of x_F at the energies of RHIC and LHC.

Relying on the standard parton model for proton-nucleus collisions, one can predict the DY cross section integrated over transverse momentum employing QCD factorization and data for the nuclear structure functions measured in deep-inelastic scattering (DIS)[1]. However, no reliable way is known to calculate nuclear effects in the transverse momentum distribution within the parton model.

Moreover, for nucleus-nucleus collisions parton model predictions are doubtful even for the integrated DY cross section. Indeed, compared to pA collisions, this case requires an additional integration over impact parameter [see Eq. (47)] and knowledge of the dependence of nuclear shadowing on impact parameter. Neither DIS, nor the DY reaction on nuclei provide such information. In principle one can access information on the impact parameter of interaction relying, for instance, on the amount of so called gray tracks and using simple cascade models. However, this possibility has never been realised for DIS or DY process. In view of this problem, it was assumed in a recent analysis [6] that nuclear shadowing is independent of impact parameter. Clearly, this cannot be correct, and it leads to confusing conclusions. In particular, the DY cross section in heavy ion collisions turns out to be independent of centrality. It is known, however, for many processes, that peripheral collisions are similar to the free NN interaction, while central collisions should manifest the strongest nuclear effects.

In this paper we calculate nuclear shadowing for the DY cross section using the light-cone (LC) dipole approach suggested in [7], which overcomes these problems in a simple way. In the rest frame of the target, the DY reaction cannot be interpreted as quark-antiquark annihilation, since it makes no sense to talk about the parton density of a proton (or a nucleus) at rest. Indeed, Feynman's picture of high energy collisions, in which the colliding particles are viewed as bunches of non-interacting partons with no (or small) transverse momenta, is applicable in a fast moving frame only. Instead, the DY process in this kinematics should be interpreted as the bremsstrahlung by a beam quark of a heavy photon, which decays into the lepton pair, as in fig. 1. Although this looks very different from the more familiar DY mechanism [8], it is known that the space-time interpretation of high-energy reactions is not Lorentz invariant and depends on the reference frame.

A quark of the incident hadron can fluctuate into a state that contains a massive photon (dilepton) and a quark. Interaction with the target breaks down the coherence of the fluc-

[1]The analysis of data [4] based on the DGLAP evolution equations still neglects effects of saturation [5] that should be important as far as shadowing sets on. Additionally, no data for DIS on nuclei are available for small Bjorken x relevant for LHC.

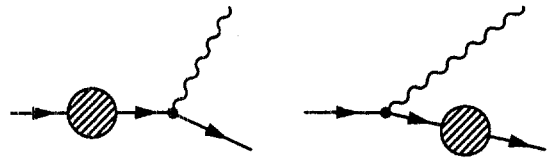

Figure 1: *In the target rest frame, DY dilepton production looks like bremsstrahlung. A quark or an anti-quark from the projectile hadron scatters off the target color field (denoted by the shaded circles) and radiates a massive photon, which subsequently decays into the lepton pair. The photon decay is not shown. The photon can be radiated before or after the quark scatters.*

tuation and the γ^* is freed. Correspondingly, the cross section of the process $qp \to \gamma^* X$ has a factorized form [7, 9, 10, 11, 12],

$$\frac{d\sigma(qp \to \gamma^* X)}{d\ln\alpha} = \int d^2\rho \, |\Psi_{\gamma^* q}(\alpha,\rho)|^2 \, \sigma^N_{\bar{q}q}(\alpha\rho, x_2) \; . \tag{1}$$

where $\Psi_{\gamma^* q}(\alpha,\rho)$ is the LC distribution amplitude in Eqs. (B.2) or (B.3) for having a quark-photon (transversely or longitudinally polarized) fluctuation with transverse separation $\vec{\rho}$ and relative fractions α and $1-\alpha$ of light-cone momenta carried by the photon and quark, respectively. For the DY reaction in pp-scattering, the dipole cross section needed in (1) is the same $\sigma^N_{q\bar{q}}$ as in DIS off a proton [2]. Note, that in the two graphs for bremsstrahlung, fig. 1, the quark scatters at different impact parameters, depending on whether it scatters when in the $|\gamma^* q\rangle$-state (right) or not (left). This leads to the appearance of the dipole cross section $\sigma^N_{q\bar{q}}(\alpha\rho, x_2)$ in (1), although there is actually no physical dipole in this process [7, 11].

We use standard kinematical variables,

$$x_1 = \frac{2P_2\cdot q}{s} \quad , \quad x_2 = \frac{2P_1\cdot q}{s}, \tag{2}$$

with $x_1 - x_2 = x_F$ and $x_1 x_2 = (M^2 + q_T^2)/s$, where P_1, P_2 and q are the four-momenta of the beam, target and the virtual photon, respectively; $M^2 = q^2$ and $\vec{q}_T$ are the dilepton invariant mass squared and transverse momentum, respectively; $s = (P_1 + P_2)^2$.

The frame dependence of the space-time interpretation of the DY process can be illustrated by the different meanings of x_1 in different reference frames: It is well known that in the standard picture of DY [8], x_1 is the momentum fraction of the projectile quark annihilating with the target antiquark. However, evaluating the scalar product (2) in the target rest frame shows that the projectile quark carries momentum fraction $x = x_1/\alpha > x_1$ of its parent hadron and, correspondingly, x_1 is the momentum fraction of the proton taken away by the photon. This is not a contradiction, since the projectile quarks in the two reference frames are different particles.

[2] This can be easily proven in leading-log order or otherwise justified by referring to QCD factorization.

In the case of a pA-scattering, one has to distinguish between two limiting kinematical regimes for the DY reaction. On the one hand, there is the regime of short coherence time t_c, which can be interpreted as the mean fluctuation lifetime. If t_c is much shorter than the mean internucleon separation no effect of coherence (shadowing) is expected. On the other hand, in the regime of long coherence time compared to the nuclear radius, $t_c \gg R_A$, interference of the multiple interaction amplitudes with bound nucleons will affect the probability of breaking down the coherence of the fluctuation and releasing the dilepton on mass shell, i.e. shadowing (sometimes antishadowing) occurs. These interferences are controlled by the longitudinal momentum transfer $q_c = 1/t_c$ in the process of γ^* radiation by a projectile quark of energy E_q, $q\,N \to \gamma^*\,q\,X$,

$$q_c = \frac{M^2_{\gamma^* q} - m_q^2}{2\,E_q}\ , \tag{3}$$

where we assume energy conservation, and the invariant mass squared of the $\gamma^* q$ pair is

$$M^2_{\gamma^* q} = \frac{M^2}{\alpha} + \frac{m_q^2}{1-\alpha} + \frac{q_T^2}{\alpha(1-\alpha)}\ . \tag{4}$$

One arrives at a similar estimate with help of the uncertainty principle. Indeed, a quark can violate energy conservation by fluctuating into $\gamma^* q$ for a time $\Delta t \sim 1/(M_{\gamma^* q} - m_q)$ in the quark's rest frame. Applying the Lorentz gamma-factor $\gamma \sim 2E_q/(M_{\gamma^* q} + m_q)$ one reproduces the lifetime $t_c = 1/q_c$ in the lab frame as given by (3).

The intuitive space-time pattern related to the coherence time for DY pair production off nuclei is rather obvious. In the limit of short coherence time (relevant for the SPS energy) the initial state interactions are predominantly soft, since the hard fluctuation containing the heavy dilepton appears only deep inside the nucleus and is momentarily freed on mass shell via the interaction with a bound nucleon.

On the other hand, if the coherence length substantially exceeds the size of the nucleus (as expected for the energies of RHIC and LHC), the hard fluctuation is created long in advance of the interaction with the nucleus, which acts as a whole in freeing the fluctuation. Since different target nucleons compete with each other, the DY cross section is subject to shadowing.

In this paper, we study nuclear effects in the limit of long coherence time. This is a most interesting regime, where interference effects are maximal and all the nucleons having the same impact parameter participate coherently in the DY process. A special advantage of the color-dipole approach is that it allows one to incorporate nuclear shadowing via a simple eikonalization of the dipole cross section $\sigma^N_{q\bar{q}}$ [13, 7] (see next section). This follows from the fact that in this limit the dipole size is "frozen" by Lorentz time dilation.

A projectile quark can develop more complicated fluctuations which besides the heavy photon also involve gluons, which correpond to Fock states $|q\gamma^* G\rangle$, $|q\gamma^* 2G\rangle$, etc. Interaction of these fluctuations with the nucleus is also affected by shadowing which may be even stronger than for the $|q\gamma^*\rangle$ one provided that the fluctuation lifetime is long compared with nuclear size. This additional shadowing in terms of parton model is related to shadowing of gluons which results from gluon fusion at small x_2 (see Sect. 3).

One might think that in the case of pA collision shadowing for DY can be easily predicted relying on QCD factorization and using data for shadowing in DIS off nuclei. However, data at small x are available only at very low Q^2 where neither factorization, nor DGLAP evolution are expected to be valid. Additionally, one should be cautious applying factorization at large x_1 where, as we pointed out above, higher twist corrections are rather large [3]. In particular, the Bjorken x of the target, x_2, reaches its minimal value as $x_1 \to 1$; therefore, factorization predicts the maximal strength for shadowing. However, shadowing for the DY process vanishes in this limit. Indeed, since $\alpha > x_1$, the invariant mass Eq.(4) increases (for massive quarks and/or nonzero q_T), leading to the disappearance of the coherence length.

We do not make any fit to the observed shadowing in DIS on nuclei, but follow the logic of the conventional Glauber approach. Namely, one is permitted to make any fits to data for nucleon-nucleon collisions, but then nuclear effects must be predicted in a parameter free way. Indeed, we use the phenomenological dipole cross section on a nucleon target [14] which is fitted to data for ep DIS from HERA, which covers a range of much higher energies than available from fixed target data for nuclear shadowing. The DY cross section calculated with this phenomenological cross section is supposed to include all higher order corrections and higher twist effects.

Another important advantage of our approach is the possibility to calculate nuclear effects in the transverse momentum distribution of DY pairs, which is a difficult problem within the parton model. The phenomenon of nuclear broadening of the dilepton transverse momentum looks very different at low (short l_c) and high (long l_c) energies. If t_c is short, the hard fluctuation containing the heavy dilepton is created deeply inside the nucleus just before the interaction, which releases it. Meanwhile, the incident hadron may have soft initial state interactions in the nucleus. These do not generate DY dileptons, but rather increase the mean transverse momentum of the fast partons of the projectile. Indeed, a fast parton experiencing multiple interactions performs a sort of Brownian motion in the plane of transverse momenta. Thus, the parton arrives with an increased transverse momentum at the point of the DY pair creation. The dilepton carries undisturbed information about the enhanced transverse momentum of the projectile quark when it is produced off a nucleus as compared to a proton target. Nuclear broadening in the limit of short coherence time was investigated previously in [15].

At first glance, in terms of parton model the observed broadening of the dilepton transverse momentum should be interpreted as a result of increase transverse momentum of quarks and antiquark in the nucleus. However, such a conclusion contradicts the usual picture of a nucleus boosted in the infinite momentum frame. Nucleons and their parton clouds are well separated and do not overlap at large x_2, the same way as they are separated in the nuclear rest frame. We know that only at very small x_2 the parton clouds overlap and fuse leading to nuclear shadowing. Such a fusion process results not only in suppressed parton density, but also in an increased transverse momenta of partons. Thus, shadowing and q_T broadening at small x_2 are closely related processes, no broadening is possible without shadowing. However, the regime of short l_c corresponds to large x_2 where neither shadowing, not q_T broadening is expected for the nuclear parton distribution function. Thus, we face a puzzle, nuclear broadening of the transverse momentum distribution of DY pairs calculated in the

nuclear rest frame and observed experimentally, has no analog withing the parton model. This puzzle has been resolved long time ago by Bodwin, Brodsky and Lepage [16] who found that in the regime of short coherence length initial state interactions leading to p_T broadening, violates QCD factorization, and should not be translated to a nuclear modification of the quark distribution function. Initial state energy loss [2, 3] also cannot be translated to a modification of x-distribution of partons in nuclei. This is a general statement which is applied to other hard reactions, like high-q_T hadron production etc.

In the regime of long coherence time $t_c \gg R_A$ relevant to RHIC and LHC, a very different mechanism is responsible for broadening of the transverse momentum distribution [10]. A high energy projectile quark emits a dilepton fluctuation (via a virtual time-like photon) long before its interaction with the nucleus. These components of the fluctuation, the recoil quark and the dilepton, do not "talk" to each other because of Lorentz time dilation. Therefore, multiple interactions of the quark in nuclear matter seem to have no further influence on the produced dilepton, *i.e.* no broadening of the transverse momentum is expected. However, this conclusion is not correct. While it is true that different ingredients of the fluctuation cannot communicate, not all fluctuations contribute to DY pair production: many (most) of them survive the interaction with the target and preserve coherence, i.e. produce no dilepton. The harder the fluctuation, i.e. the larger the intrinsic relative transverse momentum between the quark and dilepton, the stronger the kick from the target required for loss of coherence, i.e. for the fluctuation to be produced on mass shell. Since a nucleus provides a stronger transverse kick than a proton target (because of nuclear broadening of the quark transverse momentum) it is able to free fluctuations with larger intrinsic momenta. This is how the dilepton "knows" about the target and is produced off nuclei with an increased transverse momentum.

This paper is organized as follows. We explain the main ideas of the light-cone approach in the introduction. The key ingredient of this method, the universal color dipole cross section for a $q\bar{q}$ pair interacting with a nucleon, is known from phenomenology. In Sect. 2, we explain how nuclear effects are treated in the color dipole approach. In particular, we describe, how nuclear gluon shadowing has to be included along with the $q\bar{q}$-nucleus cross section. The results for gluon shadowing are presented in Sect. 3. The results of our calculations for the DY cross section in pA collisions, and predictions for RHIC and LHC, can be found in Sect. 4. Nuclear modification of the DY pair transverse momentum is calculated for the energies of RHIC and LHC in Sect. 5. We found that the so called Cronin effect, nuclear enhancement of the DY cross section at medium-large q_T, is nearly compensated at RHIC energies but is expected to have a large magnitude at LHC. We conclude that nuclear broadening of the DY transverse momentum squared diverges logarithmically for transversely polarized photons if nuclear shadowing occurs. Differences in nuclear effects for radiation of longitudinally and transversely polarized photons lead to specific nuclear modification of the DY polarization. Corresponding predictions are presented in Sect. 6. In particular, we found substantial deviation from the so called Lam-Tung relation [17]. Indeed, this relation is not supported by data, which is difficult to explain within the standard parton approach. In Sect. 7 we address the more difficult problem of nuclear effects in heavy ion collisions. We follow conventional wisdom and simplify the problem bu employing QCD factorization. Nuclear

shadowing for both sea and valence quarks is calculated within the LC dipole approach. In contrast to usual expectations, shadowing for valence quarks turns out to be larger than for the sea. We summarize the results and observations of this paper in Sect. 8 and present an outlook for further development and application of the LC dipole approach.

2 The $q\bar{q}$-nucleus cross section

In order to calculate the DY cross section in pA scattering one has to replace $\sigma_{q\bar{q}}^N$ in Eq. (1) by the color dipole cross section on a nucleus, $\sigma_{q\bar{q}}^A(\rho, x)$, which is easy to calculate within the color dipole approach.

In the limit of long coherence time, the projectile quark may be decomposed into a series of Fock-states with frozen transverse separations. Since partonic configurations with fixed transverse separations in impact parameter space are interaction eigenstates [13], $\sigma_{q\bar{q}}^A(\rho, x)$ may be calculated using Glauber theory [18], i.e. via simple eikonalization of the $q\bar{q}$-nucleon cross section,

$$\widetilde{\sigma}_{q\bar{q}}^A(\rho, x) = 2 \int d^2b \left[1 - \left(1 - \frac{1}{2A} \sigma_{q\bar{q}}^N(\rho, x)\, T_A(b) \right)^A \right], \tag{5}$$

where b is the impact parameter, A is the nuclear mass number and

$$T_A(b) = \int_{-\infty}^{\infty} dz \rho_A(b, z) \tag{6}$$

is the nuclear thickness, i.e. the integral over the nuclear density. We mark $\sigma_{q\bar{q}}^A$ in Eq. (5) with a tilde, because it still misses important contributions. We eventually motivate an improved eikonal formula Eq. (13) which incorporates the effects of higher Fock components.

The single scattering term can be obtained by expanding (5) to first order in $\sigma_{q\bar{q}}^N(\rho, x)$. The dipole interacts with the target by exchange of a gluonic colorless system, the so called Pomeron. The unitarity cut of such an amplitude reveals multiple gluon radiation which is related to higher Fock states within the LC approach in the target rest frame. Thus, for single scattering, $\sigma_{q\bar{q}}^N$ takes all Fock states of the projectile parton into account, not only $|q\bar{q}\rangle$. The energy dependence of the dipole cross section is generated by the phase space of gluons from higher Fock states $|q\bar{q}G\rangle$, $|q\bar{q}GG\rangle$, ... Indeed, in the Born approximation, i.e. two gluon exchange, $\sigma_{q\bar{q}}^N$ would be independent of x.

Calculation of $\sigma_{q\bar{q}}^N$ from first principles is still a challenge. We rely on phenomenology and employ the parametrization of Golec-Biernat and Wüsthoff [14] motivated by the saturation model,

$$\sigma_{q\bar{q}}^N(\rho, x) = \sigma_0 \left[1 - \exp\left(-\frac{\rho^2 Q_0^2}{4(x/x_0)^\lambda} \right) \right], \tag{7}$$

where $Q_0 = 1$ GeV and the three fitted parameters are $\sigma_0 = 23.03$ mb, $x_0 = 0.0003$, and $\lambda = 0.288$. This dipole cross section vanishes $\propto \rho^2$ at small distances, as implied by color transparency and levels off exponentially at large separations, which reminds one of

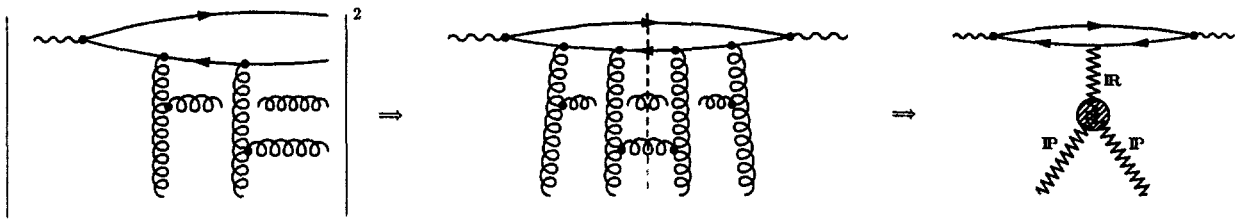

Figure 2: *The eikonal formula (5) takes only multiple rescatterings of the $|q\bar{q}\rangle$-Fock component into account. This figure illustrates the amplitude for double scattering (left). When the amplitude is squared (middle), the gluon rungs combine to gluon ladders (Pomerons), which are enclosed into each other. In Regge theory, this contribution to the cross section is expressed in terms of the Pomeron-Pomeron-Reggeon vertex (right).*

eikonalization. The authors of [14] are able to fit all available HERA data with a quite low χ^2 and can also describe diffractive HERA data.

We now turn to the multiple scattering terms. Describing shadowing for DY is simplified if we make use of the fact that the dipole cross section entering the formula for dilepton production Eq. (1) is the same that is needed to calculate the DIS cross section. We may thus illustrate the physics of Eq. (5) in fig. 2, where the double scattering term for a $q\bar{q}$-dipole is depicted. In terms of Regge phenomenology, the double scattering of the $q\bar{q}$-pair corresponds to the Pomeron-Pomeron-Reggeon vertex. Note that (5) does not only account for the double scattering term, but also for all higher order rescatterings of the $q\bar{q}$-pair. The n-fold scattering graph has n gluon ladders, which are enclosed into each other.

Rescatterings of higher Fock states, containing gluons are omitted in (5). At low x, however, the lifetime of these higher Fock states will become significantly longer than the mean internucleon distance and they will scatter more than once inside the nucleus, as illustrated in fig. 3. In this case, which occurs at RHIC and LHC energies, (5) needs to be modified to include also these rescattering.

In order to include processes like the one illustrated in fig. 3, it is useful to note that the rescattered gluon can be interpreted as the first rung of a single gluon ladder exchanged between the $q\bar{q}$-pair and the target. In Regge phenomenology, rescattering of gluons leads to the triple-Pomeron vertex fig. 3(right), which can be regarded as a correction to the single scattering term. More precisely, it leads to a reduction of the nuclear gluon density, because the two Pomerons from the target in fig. 3(right) fuse to a single one, before interaction with the pair. Indeed, multiple scatterings of higher Fock states containing gluons are known as the effect of gluon shadowing [19] and lead to an additional suppression of the DY cross section. In the infinite momentum frame of the nucleus gluon clouds of different nucleons overlap and fuse at small x [20, 5], fig. 3(right), thereby reducing the gluon density at small x. Although the corrections for gluon rescatterings (in the nuclear rest frame) and gluon fusion (in the nuclear infinite momentum frame) look very different, this is the same phenomenon seen from different reference frames. Of course, observables are Lorentz invariant, and both

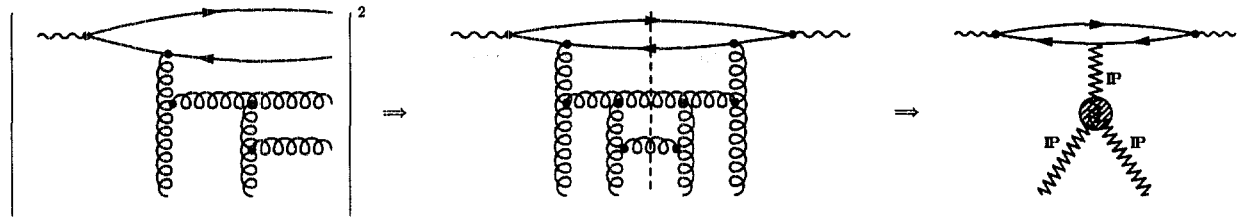

Figure 3: *At high energy, the lifetime of higher Fock states becomes long enough for multiple scattering. Shown here is the double scattering amplitude for the $|q\bar{q}G\rangle$-Fock state. In Regge theory, this process is expressed in terms of the triple-Pomeron vertex (right). The eikonal formula (5) is improved to include also these contributions, by multiplying $\sigma_{q\bar{q}}$ with the gluon shadowing ratio R_G, Eq. (13).*

effects lead to a reduction of the DY cross section.

Thus, the Pomeron-Pomeron fusion process in fig. 3(right) can be taken into account by multiplying $\sigma^N_{q\bar{q}}(\rho, x)$ with the gluon shadowing ratio

$$R_G(x, \widetilde{Q}^2,) = \frac{G_A(x, \widetilde{Q}^2)}{AG_N(x, \widetilde{Q}^2)} = 1 - \Delta R_G(x, \widetilde{Q}^2). \tag{8}$$

The single scattering term reads then

$$\begin{aligned} \sigma^A_{q\bar{q}}(x, \rho) &= \sigma^N_{q\bar{q}}(\rho, x) \int d^2b R_G(x, \widetilde{Q}^2, b) T_A(b) + \ldots, \\ &= A\sigma^N_{q\bar{q}}(\rho, x) \left[1 - \frac{1}{A} \int d^2b \Delta R_G(x, \widetilde{Q}^2, b) T_A(b)\right] + \ldots, \end{aligned} \tag{9}$$

where we calculate gluon shadowing as function of impact parameter b. The first term in (9) stands for direct exchange of a Pomeron, while the second, negative term represents the correction due to the Pomeron fusion process depicted in fig. 3. This recipe becomes even more clear from the relation valid at $\rho \to 0$ [21],

$$\sigma^N_{q\bar{q}}(\rho, x)\Big|_{\rho \to 0} = \frac{\pi^2}{3} \alpha_s \left(\frac{\lambda}{\rho^2}\right) \rho^2 \, G_N \left(x, \frac{\lambda}{\rho^2}\right). \tag{10}$$

In (9), the proton gluon density in (10) was replaced by the average nuclear gluon density,

$$\sigma^N_{q\bar{q}}(\rho, x)\Big|_{\rho \to 0} \Rightarrow \frac{\pi^2}{3} \alpha_s \left(\frac{\lambda}{\rho^2}\right) \rho^2 \, \frac{1}{A} \, G_A \left(x, \frac{\lambda}{\rho^2}\right). \tag{11}$$

It is clear from (9) that the effective dipole cross section on a bound nucleon appears to be reduced due to gluon shadowing. We also see from (10) that R_G has to be evaluated at a scale $\widetilde{Q}^2 = \lambda/\rho^2$.

What fusion processes are included in (9) depends on the approximation in which gluon shadowing R_G is evaluated. For our actual calculations (see Sect. 3) nuclear shadowing for gluons is calculated within the Green function formalism for a $|q\bar{q}G\rangle$ fluctuation propagating through nuclear medium developed in [22]. This means, that the single scattering term in (9) is corrected not only for the $2\mathbb{P} \to \mathbb{P}$ Pomeron fusion term depicted in fig. 3(right), but also all the $n\mathbb{P} \to \mathbb{P}$ fusion processes are taken into account. Moreover, the Green function approach properly describes the finite lifetime of the $|q\bar{q}G\rangle$-state. This is important, because even when the $q\bar{q}$-fluctuation lives much longer than the nuclear radius, the lifetime of the $|q\bar{q}G\rangle$-state will be shorter.

For the rescattering terms, we can account for higher Fock states in the same way as in (9), namely by the replacement [23, 24]

$$\sigma_{q\bar{q}}^N(\rho, x) \Rightarrow \sigma_{q\bar{q}}^N(\rho, x) R_G(x, \widetilde{Q}^2, b) \ , \tag{12}$$

i.e. the improved formula Eq. (5) for the $q\bar{q}$-nucleus section reads,

$$\sigma_{q\bar{q}}^A(\rho, x) = 2 \int d^2b \left[1 - \left(1 - \frac{1}{2A} \sigma_{q\bar{q}}^N(\rho, x) R_G(x, \lambda/\rho^2, b) T_A(b) \right)^A \right] . \tag{13}$$

This expression includes also the contribution of higher Fock states containing more than one gluon. The higher order multiple interactions of the $|q\bar{q}G\rangle$ Fock state correspond, as was mentioned, to multi-Pomeron fusion, $n\mathbb{P} \to \mathbb{P}$, while the Reggeon diagrams with $n\mathbb{P} \to m\mathbb{P}$ $(m \geq 2)$ are missing. Those diagrams should be incorporated via the Fock components $|q\bar{q}\, mG\rangle$ containing two or more gluons. The modified expression Eq. (13) sums multiple interactions of the $q\bar{q}$ pair via $m\mathbb{P}$ exchange (summed over m) each of which has a form of a fan $n\mathbb{P} \to \mathbb{P}$ (summed over n). We assume that each gluon in the Fock state $|q\bar{q}\, mG\rangle$ experiences multiple interactions independently of other gluons. This assumption correspond to the Gribov's interpretation [25] of the Glauber eikonal shadowing, namely the unitarity cut of an n-fold scattering term must contain a simultaneous cut of all n Pomerons. Therefore it corresponds to nonplanar graph describing independent multiple interaction of n projectile partons (see discussion in [24]).

We can now proceed to calculate $\sigma_{q\bar{q}}^A(x, \rho)$ according to (13). We briefly summarize our calculation of gluon shadowing (R_G) [22] in section 3. The results for the nuclear dipole cross section $\sigma_{q\bar{q}}^A(\rho, x)$ are depicted in fig. 4. Since (13) is a high energy approximation valid when the lifetime of the $q\bar{q}$-pair exceeds the nuclear radius, these results are relevant at RHIC and LHC energies. At lower energies however, one has to take transitions between different eigenstates into account [10].

The plot on the l.h.s. of fig. 4 shows the dipole cross section itself. First, we discuss the $q\bar{q}$-proton cross section. The two upper curves show this quantity for two different values of x typical for RHIC and LHC. After a quadratic rise $\sigma_{q\bar{q}}^N$ levels off and takes an energy independent saturation value of 23.03 mb. The onset of saturation, i.e. the flattening of the dipole cross section as function of ρ is controlled by the saturation radius,

$$R_s^2(x) = \frac{2}{Q_0^2} \left(\frac{x_0}{x} \right)^\lambda , \tag{14}$$

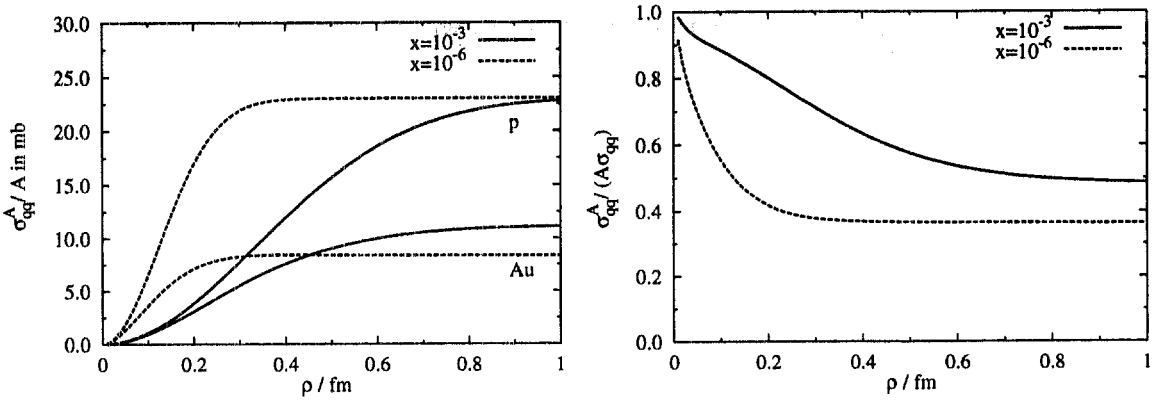

Figure 4: *The figure on the left shows the $q\bar{q}$-nucleus cross section (13) divided by the nuclear mass number A for two different values of x. The two lower curves (solid and dashed) are calculated for gold ($A = 197$) and the two upper curves for a proton. The figure on the right shows the $q\bar{q}$-nucleus cross section divided by A times the dipole cross section (7). While large separations are strongly suppressed, small size dipoles are much less affected by the nucleus. Nuclear gluon shadowing is included in the calculation, as explained in the text. It vanishes at small $q\bar{q}$ separations which correspond to high Q^2.*

which decreases with energy. The energy dependence of (7) correlates with ρ. At $\rho \ll R_s$ the dipole cross section grows with a hard Pomeron intercept $\lambda = 0.288$ with energy, while at large separations, $\rho \gg R_s$, (7) becomes independent of energy. For more discussion on (7) we refer to the original work [14].

We now turn our attention to the $q\bar{q}$ nucleus cross section $\sigma^A_{q\bar{q}}(\rho, x)$, eq. (13), which is shown by the two lower curves in fig. 4 (left). In addition to the expected suppression due to nuclear shadowing, one also sees that the saturation value of $\sigma^A_{q\bar{q}}$, which is approximately at its geometrical limit $2\pi R_A^2$, is energy dependent. Moreover, $\sigma^A_{q\bar{q}}(\rho \to \infty, x)$ is a decreasing function of energy. This is a consequence of the gluon shadowing in (13). At very small x, gluon shadowing becomes strong, (see fig. 6) and the $q\bar{q}$ nucleus cross section lies below its geometrical limit. The stronger the gluon shadowing, the smaller the saturation value of $\sigma^A_{q\bar{q}}$. However, $R_G \to 1$ at $\rho \to 0$ since $Q^2 \sim 1/\rho^2 \to \infty$ (see fig. 6).

The nuclear suppression of the dipole cross section is plotted on the right of fig. 4. Small sizes are less affected by the nucleus than large sizes. This illustrates the effect of color filtering [26], which is the mechanism behind nuclear broadening of transverse momenta (see section 5). While small $q\bar{q}$-pairs, which have large intrinsic transverse momenta according to the uncertainty principle, propagate through the nucleus almost undisturbed, large pairs (small transverse momenta) are absorbed, i.e. the coherence of the fluctuation is disturbed and the γ^* is freed. Absorption thus leads to an increase of the mean transverse momentum.

3 Gluon shadowing in nuclei

The nuclear shadowing for gluons needed as input for the $q\bar{q}$-nucleus cross section in (13) is calculated in the LC Green function approach developed in [22], where gluon shadowing is calculated from shadowing of the $|q\bar{q}G\rangle$ Fock-component of a longitudinally polarized photon. In this section, we briefly review the approach of [22] and present the results of our calculation for gluon shadowing as function of x, Q^2 and the length L of the path in the nuclear medium.

Longitudinal photons can serve to measure the gluon density because they effectively couple to color-octet-octet dipoles. This can be understood in the following way: The light-cone wave function for the transition $\gamma_L^* \to q\bar{q}$ does not allow for large, aligned jet configurations. Thus, unlike the transverse case, all $q\bar{q}$ dipoles from longitudinal photons have size $1/Q^2$ and the double scattering term vanishes like $\propto 1/Q^4$. The leading twist contribution for the shadowing of longitudinal photons arises from the $|q\bar{q}G\rangle$ Fock state of the photon. Here again, the distance between the q and the $\bar{q}$ is of order $1/Q^2$, but the gluon can propagate relatively far from the $q\bar{q}$-pair. In addition, after radiation of the gluon, the pair is in an octet state. Therefore, the entire $|q\bar{q}G\rangle$-system appears as a GG-dipole, and the shadowing correction to the longitudinal cross section is just the gluon shadowing we want to calculate.

A critical issue for determining the magnitude of gluon shadowing is the distance the gluon can propagate from the $q\bar{q}$-pair in impact parameter space, i.e. knowing how large the GG dipole can become. In [22], this value was able to be extracted from single diffraction data in hadronic collisions because these data allow one to unambiguously single out diffractive gluon radiation (the triple-Pomeron contribution in Regge phenomenology). The diffraction cross section ($\propto \rho^4$) is even more sensitive to the dipole size than the total cross section ($\propto \rho^2$) and is therefore a sensitive probe of the mean transverse separation. It was found in [22] that the mean dipole size must be of the order of $r_0 = 0.3$ fm, considerably smaller than a light hadron. A rather small gluon cloud of this size surrounding the valence quarks is the only way known to resolve the long-standing problem of the smallness of the triple-Pomeron coupling. The smallness of the GG dipole is incorporated into the LC approach by a nonperturbative interaction between the gluons.

Note that the small value of r_0 dictated by data for diffraction is consistent with the results of other approaches. Indeed, the same small size characterizing gluonic fluctuations was found in the instanton liquid model [27] and in the QCD sum rule analysis of the gluonic formfactor of the proton [28], and it also follows from lattice calculations [29]. Note that the value of r_0 also limits the Q^2-range where the approximation $q\bar{q}G \approx GG$ is valid. One has to ensure that $Q^2 \gg 1/r_0^2$, otherwise the $q\bar{q}$ pair is not pointlike compared to the size of the entire Fock state.

Our results for gluon shadowing as a function of the length of the path in the nuclear medium are shown in fig. 5. The calculations are performed for lead with a uniform nuclear density of $\rho_A = 0.16$ fm^{-3}. Details are presented in Appendix A. The small size of the GG dipole leads to a rather weak gluon shadowing (except for specific reactions where the $q\bar{q}$ pair is colorless [24]). For most values of x, gluon shadowing increases as a function of L as one

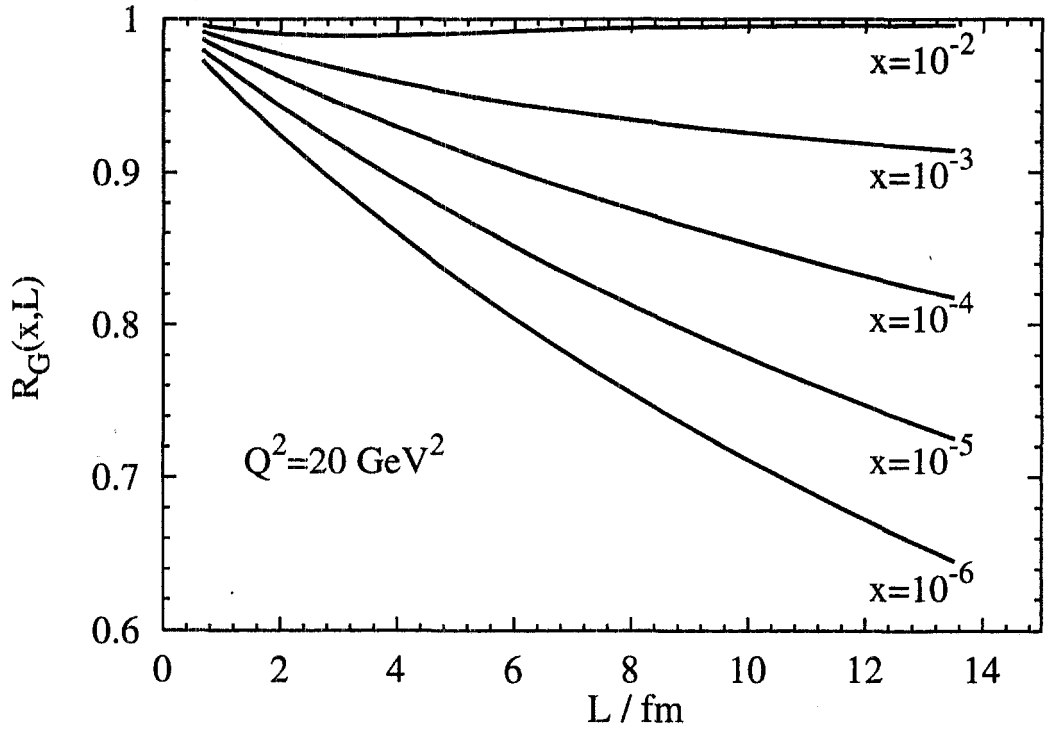

Figure 5: *Gluon shadowing vs. the length of the nuclear medium* $L = 2\sqrt{R_A^2 - b^2}$. *All curves are for* $Q^2 = 20\ GeV^2$, *but for different values of* x.

would expect. At the largest value of $x = 0.01$, however, gluon shadowing becomes smaller as L increases and R_G approaches 1. Although this behavior seems to be counterintuitive, it can be easily understood by noting that at $x = 0.01$ the coherence length of the $|q\bar{q}G\rangle$-Fock state becomes very small and the formfactor of the nucleus supresses shadowing [30]. The curves shown in fig. 5 are the ones which actually enter our calculation for DY via the $q\bar{q}$-nucleus cross section (13). The values of x entering our calculation are $x \approx 10^{-3}$ for RHIC and $x \approx 10^{-6}$ for LHC.

We also calculate gluon shadowing as function of x at fixed Q^2 and as a function of Q^2 at fixed x, integrated over the impact parameter b. The results are shown in fig. 6. In the left plot, one observes that gluon shadowing vanishes for $x > 0.01$. This happens because the lifetime of the $|q\bar{q}G\rangle$-fluctuation becomes smaller than the mean internucleon distance of ~ 2 fm as x exceeds 0.01. Indeed, in [30] an average coherence length of slightly less than 2 fm was found for the $|q\bar{q}G\rangle$-state at $x = 0.01$ and large $Q^2 \gg 1/r_0^2$. Note that gluon shadowing sets in at a smaller value of x than quark shadowing because the mass of a $|q\bar{q}G\rangle$-state is larger than the mass of a $|q\bar{q}\rangle$-state. This delayed onset of gluon shadowing was already found in [22]. We also point out that gluon shadowing is even weaker than quark shadowing in the x-range plotted, because the small size of the GG-dipole overcompensates

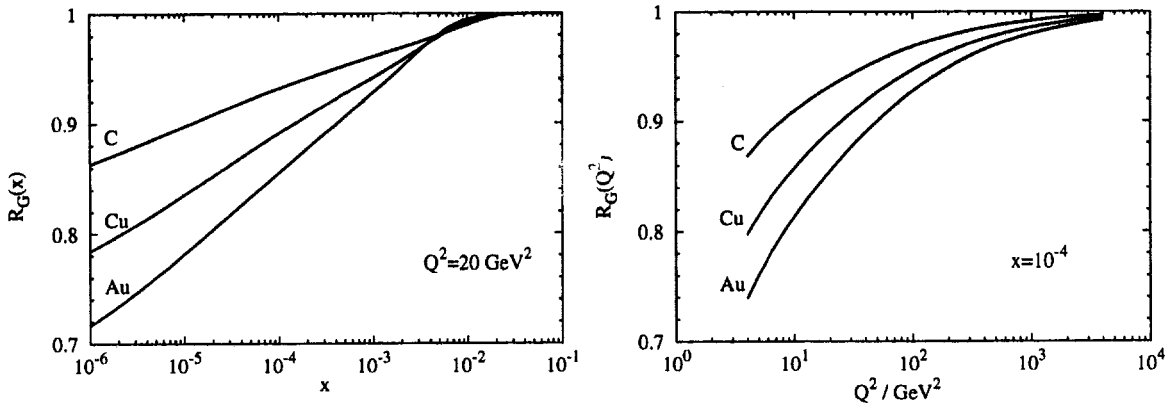

Figure 6: *The x- and Q^2-dependence of gluon shadowing for carbon, copper and gold. The x-dependence is shown for $Q^2 = 20\ GeV^2$, while the figure on the right is calculated for $x = 10^{-4}$.*

the Casimir factor in the GG-proton cross section, $\sigma^N_{GG} = (9/4)\sigma^N_{q\bar{q}}$. The plot on the right of fig. 6 shows the Q^2-dependence of gluon shadowing and clearly demonstrates that gluon shadowing is a leading twist effect. R_G only very slowly (logarithmically) approaches unity as $Q^2 \to \infty$.

4 Nuclear shadowing for DY pair production in pA- and DA-collisions

Nuclear shadowing for the DY process was first observed in proton-nucleus (pA) collisions by the E772 experiment at large x_F [1]. The shadowing effect will also be present in the energy range of RHIC and LHC. Since RHIC will probably first measure the DY cross section from deuterium-nucleus (DA) rather than pA collisions, we perform calculations for both, pA and DA collisions.

The dipole formulation provides the following explanation of shadowing in the DY process. When the coherence length is long, one of the projectile quarks develops a $\gamma^* q$-fluctuation long before it reaches the target. If the transverse momentum transfer from the target is large enough to resolve the fluctuation, the virtual photon is freed and eventually is observed as a lepton pair in the detector. In the case of a nuclear target, the set of struck nucleons compete to free the virtual photon. If the $|\gamma^* q\rangle$-state has a very small transverse size, it can propagate through the entire nucleus because none of the bound nucleons can provide a kick strong enough to resolve the $|\gamma^* q\rangle$ structure in the incident quark. These small fluctuations have the same small probability to interact with any nucleon, so they will not be shadowed. On the other hand, if the fluctuation is large in size, only a small momentum transfer is necessary to resolve the photon. Thus, the coherence of a large fluctuation will be destroyed with high probability already in the first collision on the surface of the nucleus. Nucleons deeper in the nucleus do not add much to the probability of freeing

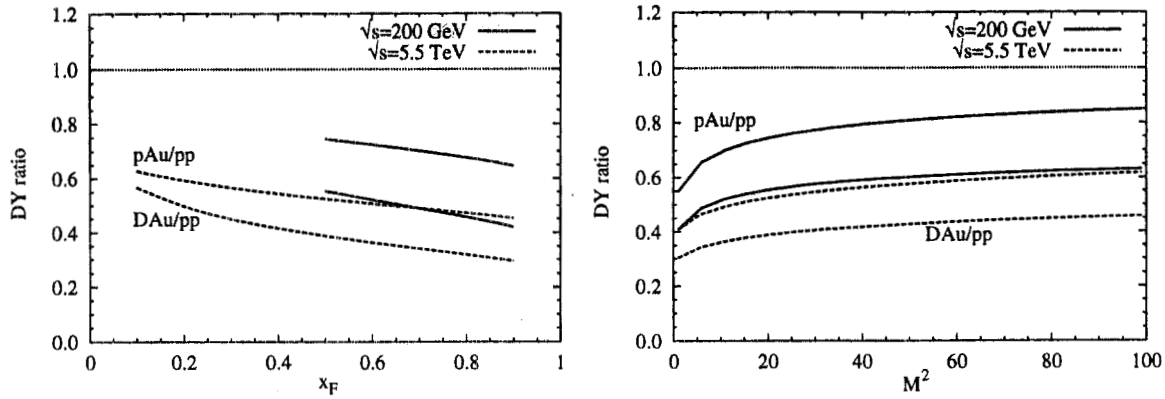

Figure 7: *Shadowing for the total DY cross section in proton – gold (upper curves) and deuterium – gold (lower curves) collisions at the energies of RHIC and LHC as function of Feynman x_F and dilepton mass M^2, respectively. The left figure is calculated for $M = 4.5$ GeV. The figure on the right for $x_F = 0.5$.*

the γ^*. Thus, this probability nearly saturates for these extremely large fluctuations, and the DY cross section will scale like $A^{2/3}$. From these considerations, we can find two necessary conditions for shadowing [30],

- The $\gamma^* q$ fluctuation must have a lifetime long enough to allow for at least two scatterings during the coherence time t_c.
- The $\gamma^* q$ fluctuation must have a large freeing cross section[3], i.e. its transverse size must be sufficiently large.

The first condition is assumed to be fulfilled throughout this paper, where we consider only the case of infinite t_c. The dependence of shadowing on the fluctuation size is encoded in the $q\bar{q}$-nucleus cross section (13).

Note that since the $\gamma^* q$-fluctuation is formed long before the target, the dilepton is unaffected by the quark energy loss. Thus, the entire suppression of the DY cross section at very low x_2, say $x_2 < 0.001$, is due to shadowing and we do not need to worry about energy loss. This is different at the lower fixed target energies [1], where the observed depletion of the DY cross section originates from a combination of shadowing and energy loss [2, 3]. The complimentary behavior of shadowing and energy loss is discussed in more detail in [3]: Long t_c means that only shadowing occurs, while for short t_c, one observes only energy loss.

To obtain the cross section for an incident hadron, the partonic cross section (1) has to be weighted with the quark (and antiquark) distributions, $q(x)$, of the projectile hadron, and

[3]One should distinguish between the freeing and the total cross sections of a fluctuation. The latter is always large for a colored quark and all its fluctuations, while the former is driven by the difference between scattering amplitudes of different fluctuations ($|q\rangle$ and $|q\gamma^*\rangle$ in our case). Since it is only the quark that interacts in each of these Fock states, the freeing cross section is controlled by the relative transverse displacement of the quarks within different fluctuations. This is how the dipole cross section comes about.

one has to include the factors necessary to account for the decay of the virtual photon into the dilepton. For an incident proton, this cross section becomes

$$\frac{d^4\sigma(pA \to l\bar{l}X)}{dM^2\,dx_F} = \frac{\alpha_{em}}{3\pi M^2}\frac{x_1}{x_1+x_2}\int_{x_1}^1 \frac{d\alpha}{\alpha^2}\sum_f Z_f^2\left\{q_f\left(\frac{x_1}{\alpha},M^2\right)+q_{\bar{f}}\left(\frac{x_1}{\alpha},M^2\right)\right\} \times\frac{d\sigma(qA\to\gamma^*X)}{d\ln\alpha}, \quad (15)$$

where Z_f is the charge of a quark of flavor f. We assume that the the same expression (15) applies for both proton and deuteron projectiles, so that the only difference between these cases is that the flavor sum ranges over the quarks of the proton *and* neutron in the case of an incident deuteron. Nuclear in the deuterium structure function and finite-size effects are neglected, and isospin symmetry is assumed.

For a calculation that actually can be compared to data, we employ the CTEQ5L parameterization [31] (taken from CERNLIB [32]) for $q_{f,\bar{f}}$. Note that since the projectile quark distributions enter at large $x = x_1/\alpha > x_1$, where they are well known. THus, the uncertainty arising from the choice of parton distributions is minimal. However, these parton distributions are different for the proton and deuterium, so that the pA and DA DY cross section are not trivially related. Shadowing can now be obtained by evaluating (15) and (1), with $\sigma^A_{q\bar{q}}(\rho,x_2)$ taken from (13), and dividing by A times the analogous calculation with the $q\bar{q}$-proton cross section (7). In the case of the deuterium projectile, we divide by $2A$. The nuclear density parametrizations are taken from [33].

The result as function of x_F and dilepton mass M at different energies is shown in fig. 7. For each energy (RHIC and LHC) we calculated pAu and DAu collisions and normalized both to pp collisions. Note that the DAu curve is always below the pAu curve (for a given energy). This is because of the different flavor structure of deuterium and the fact that d-quarks are weighted with a factor $Z_d^2 = 1/9$ in (15), compared to the factor $Z_u^2 = 4/9$ for u-quarks. For the RHIC energy of $\sqrt{s} = 200$ GeV, we calculate only for $x_F > 0.5$ to make sure that the fluctuation lifetime significantly exceeds the nuclear radius. At the very high LHC energy of $\sqrt{s} = 5.5$ TeV, the coherence time is much larger than the nuclear radius for any value of x_F (except at the very endpoints). Thus, the entire x_F-range is shadowed. Shadowing is especially strong at LHC energies at large x_F, where x_2 can become as low as $x_2 \approx 10^{-6}$. At such low x_2, the effects of gluon shadowing leads to a sizeable additional suppression of the DY cross section. Without the gluon shadowing contribution in (13), shadowing of the DY reaction at LHC would be strongly underestimated. The mass dependence of shadowing in DY is shown in the plot on the right of fig. 7. The weak dependence on M reflects the fact that shadowing for DY is a leading twist effect, just as for DIS. Indeed, configurations with $\alpha \to 1$ in (1), (15) are the analog of Bjorken's aligned jet configurations in DIS [9], which make shadowing persist as $M \to \infty$.

We also investigate the A and the impact parameter dependence of shadowing, with the results shown in fig. 8. The amount of shadowing, *i.e.* the difference from unity in fig. 8, is to a good approximation proportional to $A^{1/3}$. The deuterium curves in fig. 8 do not of course go to unity at $A = 1$ or $b \to \infty$; the flavor suppression remains in these limiting cases.

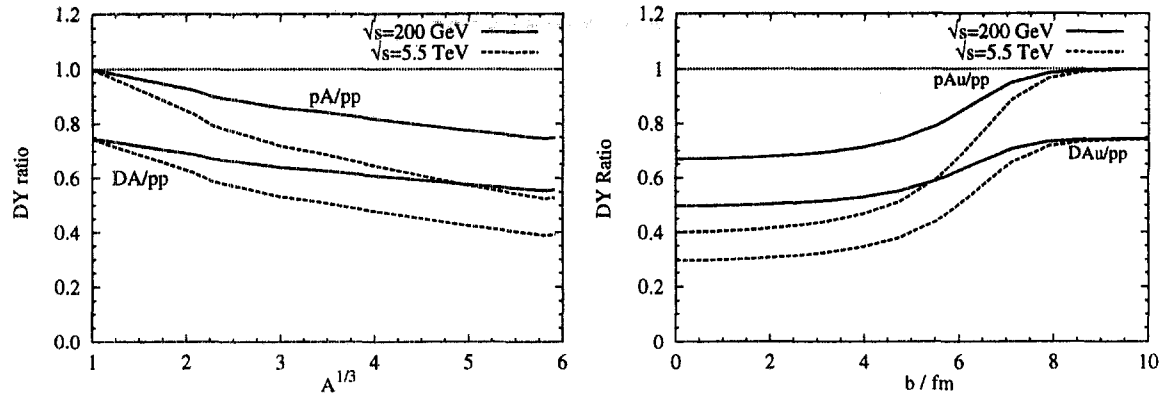

Figure 8: *Shadowing for the total DY cross section as a function of $A^{1/3}$ and impact parameter b. Both figures are calculated for $M = 4.5$ GeV and $x_F = 0.5$. In each plot, the lower pair of curves is for deuterium - gold scattering (DAu) and the two upper curves are for proton - gold collisions (pAu).*

We point out that it is a special advantage of the dipole approach that it naturally predicts the impact parameter dependence of nuclear effects. To obtain the b dependence, one simply eliminates the b integral in (13) and divides by the nuclear thickness $T(b)$ instead of A.

5 Nuclear modification of the DY transverse momentum distribution in pA- and DA-collisions

The differential DY cross section as a function of the transverse momentum q_T can be calculated in the dipole formulation as well. At the energies relevant for RHIC and LHC, the transverse momentum distribution of DY pairs from $p(D) + A$ collisions can be written in frozen approximation [10, 11],

$$\frac{d^4\sigma(pA \to l\bar{l}X)}{dM^2\, dx_F\, d^2q_T} = \frac{\alpha_{em}}{3\pi M^2}\frac{x_1}{x_1+x_2}\int_{x_1}^1 \frac{d\alpha}{\alpha^2}\sum_f Z_f^2\left\{q_f\left(\frac{x_1}{\alpha}\right) + q_{\bar{f}}\left(\frac{x_1}{\alpha}\right)\right\}\frac{d\sigma(qA \to \gamma^* X)}{d\ln\alpha\, d^2q_T}, \tag{16}$$

in analogy to Eq. (15). The differential cross section for a heavy photon radiation in a quark-nucleus collision was derived in [10],

$$\begin{aligned}\frac{d\sigma(qA \to \gamma^* X)}{d\ln\alpha d^2q_T} &= \frac{1}{(2\pi)^2}\int d^2\rho_1 d^2\rho_2\, \exp[i\vec{q}_T\cdot(\vec{\rho}_1-\vec{\rho}_2)]\Psi^*_{\gamma^* q}(\alpha,\vec{\rho}_1)\Psi_{\gamma^* q}(\alpha,\vec{\rho}_2) \\ &\times \frac{1}{2}\Big[\sigma^A_{q\bar{q}}(\alpha\rho_1,x_2) + \sigma^A_{q\bar{q}}(\alpha\rho_2,x_2) - \sigma^A_{q\bar{q}}(\alpha|\vec{\rho}_1-\vec{\rho}_2|,x_2)\Big]. \end{aligned} \tag{17}$$

Integrating this expression over q_T we arrive at the cross section Eq. (1). Three of the four integrations in (17) can be performed analytically for an arbitrary form of the dipole cross

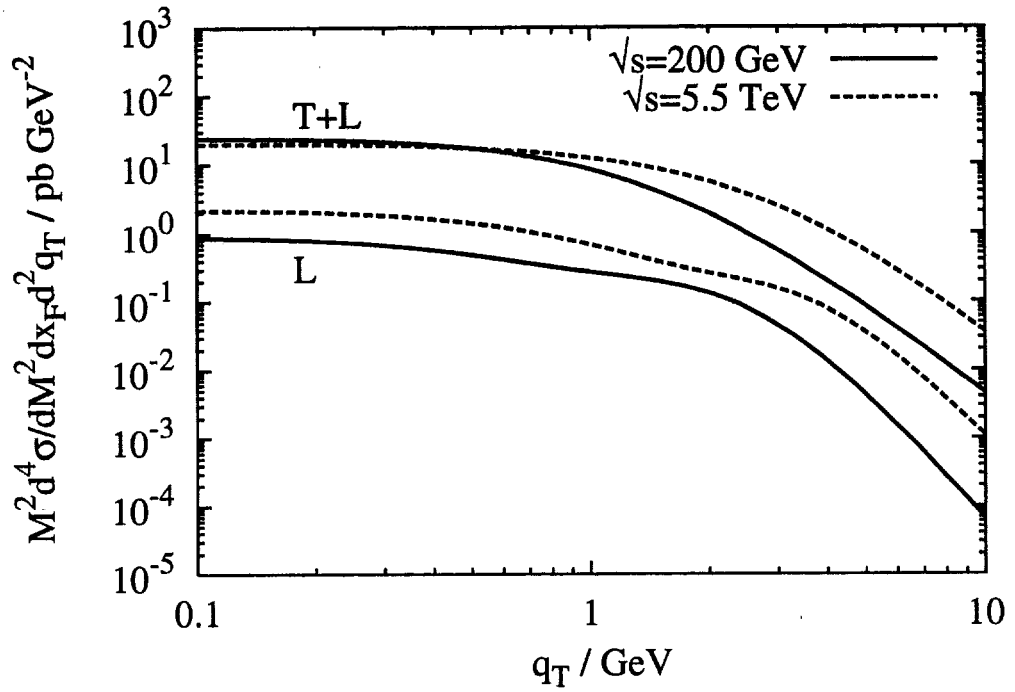

Figure 9: *Absolute value of the differential DY cross section for pAu scattering, divided by* $A(= 197)$. *The curves are predictions for RHIC* ($\sqrt{s} = 200$ *GeV) and LHC* ($\sqrt{s} = 5.5$ *TeV) for the dilepton mass of* $M = 4.5$ *GeV and* $x_F = 0.5$. *The upper two curves show the sum of transverse and longitudinal cross section* $(T + L)$ *and the lower two curves* (L) *separately show the longitudinal cross section.*

section $\sigma_{q\bar{q}}^N$ [34]. The details of calculations are moved to Appendix B. Since the remaining integration still has to be performed over an oscillating function, the q_T-range in which numerical calculations are feasible is limited. We calculate up to $q_T = 10$ GeV, which covers the experimentally interesting region.

As in the preceding section, we perform calculations for pA and for DA scattering. Our result for the differential DY cross section for transverse and longitudinal pairs are shown in fig. 9. We show only curves for pA in this figure, because the difference between pA and DA is hardly visible on the logarithmic scale. As already observed in [11], the differential cross section does not diverge at zero transverse momentum, because of the flattening of the dipole cross section at large separations. On the partonic level, we reproduce the same asymptotic behavior that is expected in the standard parton model,

$$\frac{d\sigma_T(qp \to \gamma^* X)}{d^2q_T} \propto \frac{1}{q_T^4} \quad \text{for } q_T \to \infty \tag{18}$$

and

$$\frac{d\sigma_L(qp \to \gamma^* X)}{d^2 q_T} \propto \frac{1}{q_T^6} \quad \text{for } q_T \to \infty. \tag{19}$$

Embedding the partonic cross section (17) into the hadronic environment as in (16) will lead to a somewhat steeper decay at large q_T, because x_1 increases with q_T and so the structure function F_2 of the projectile will decrease. However, even at $q_T = 10$ GeV, the asymptotic limit is not yet fully reached. The q_T dependence is still slightly less steep than in (18).

To see the effect of nuclear shadowing and antishadowing we divide the nuclear differential cross section by A times that of the nucleon ($2A$ for DA scattering). Then, nuclear effects manifest themselves as a deviation from unity. The results of calculations (see Appendix B) for gold at the energies of RHIC and LHC are presented in fig. 10 for the unpolarized (top) and longitudinally polarized (bottom) DY cross section ratios. Also, the difference between pA (left) and DA (right) now becomes clearly visible. As already explained in Sect. 4, this difference is due to the larger abundance of d-quarks in deuterium. Note that we neglected nuclear effects in deuterium and assumed isospin symmetry for the DA curves.

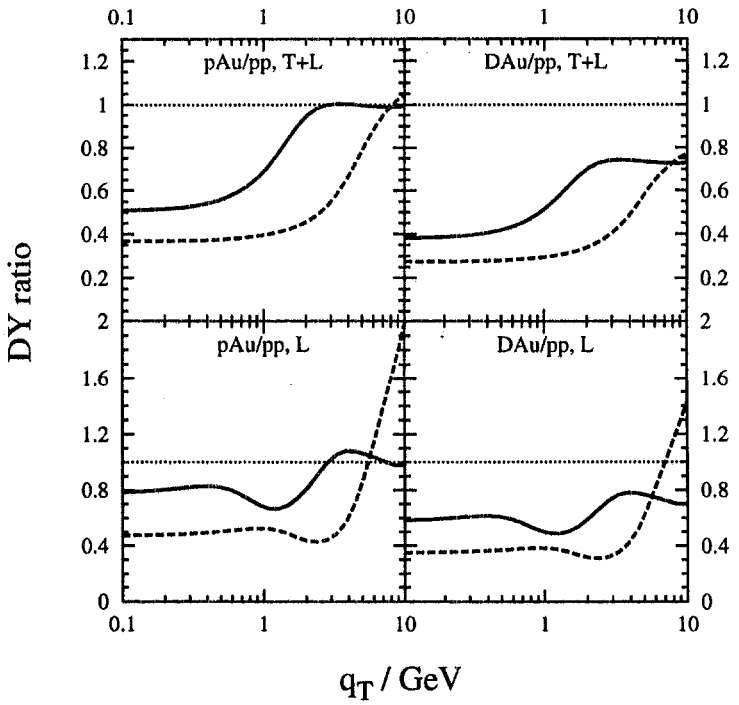

Figure 10: *Nuclear effects on the DY transverse momentum distribution. Curves show the DY cross sections for pAu (left) and deuterium - gold (right) collisions divided by A(= 197) (or $2A$ for DAu collisions, respectively) times the DY cross section from pp scattering. Solid curves are predictions for RHIC ($\sqrt{s}$ = 200 GeV) and dashed for LHC ($\sqrt{s}$ = 5.5 TeV) Calculations are for the same kinematics as fig. 9.*

For low transverse momenta, we expect DY dilepton production to be shadowed. Note that shadowing for longitudinal $\bar{q}q$ pairs is smaller than for transverse pairs because the longitudinal cross section is dominated by small distances in the dipole cross section. However, gluons shadowing which onset we observe at RHIC and which becomes the dominant effect at RHIC is about the same. Indeed, we predict rather different shadowing effects for longitudinal and transverse dileptons at RHIC, but about the same at LHC.

It is interesting that the effect of antishadowing, the so-called Cronin effect predicted in [10], disappears at the energy of RHIC after inclusion of gluon shadowing, which was disregarded in [10]. This reminds one of the missing Cronin enhancement in charged particle multiplicities that was measured at RHIC [35]. However, the RHIC data cannot be explained by gluon shadowing, because the x of the data is too large. Some antishadowing is still possible at large $q_T \sim 10$ GeV at the energy of LHC as a result of the substantial rise of the dipole cross section with energy and the corresponding relative enhancement of the multiple interactions responsible for the Cronin effect. This expectation is confirmed by fig. 11, which shows the results of calculations without (dashed curves) and with (solid) gluon shadowing.

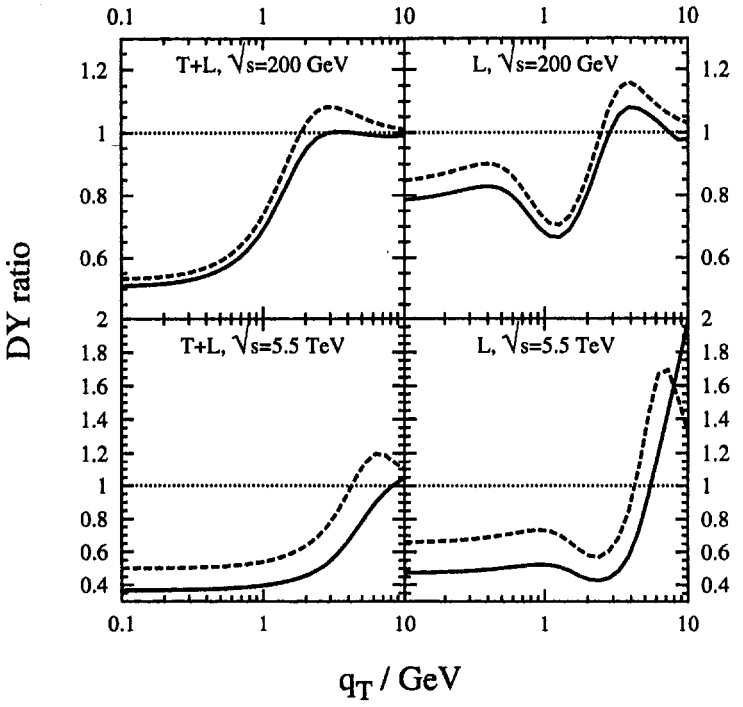

Figure 11: *The influence of gluon shadowing on the DY cross section. Dashed curves are calculated without gluon shadowing, i.e. $R_G = 1$ in (13), while solid curves include gluon shadowing. The influence on the longitudinal DY cross section is shown separately in the two left plots (L). The two plots on the right show the DY ratio for the sum of the transverse and longitudinal cross sections ($T + L$). Calculations are for the same kinematics as fig. 9.*

The DY process with the production of a longitudinally polarized photon manifests stronger effects of antishadowing (fig. 10 bottom and fig. 11 right), as was earlier observed in [10]. However, this enhancement of the longitudinal cross section will hardly be visible in experiments because the transverse cross section is so much larger than the longitudinal one. All nuclear effects are expected to vanish at very large q_T.

One can also study the moments of the transverse momentum distribution. A frequently measured characteristic of nuclear effects is the broadening of the mean value of the DY transverse momentum squared, which is the difference between the values of mean transverse momentum squared measured in pA and pp collisions,

$$\delta\langle q_T^2\rangle = \langle q_T^2\rangle_A - \langle q_T^2\rangle_N \ , \tag{20}$$

where

$$\langle q_T^2 \rangle_{A(N)} = \frac{\int_0^{q_T^{max}} d^2q_T \, q_T^2 \, d\sigma_{DY}^{pA} dq_T}{\int_0^{q_T^{max}} d^2q_T \, d\sigma_{DY}^{pN}/d^2q_T} \,. \tag{21}$$

$d\sigma_{DY}^{pA}/dq_T$ is the proton-nucleus DY cross section given by Eq. 16.

It is easy to understand from fig. 10, that a nuclear target leads to a larger mean transverse momentum of DY dileptons than a proton target: Low q_T pairs, corresponding to large arguments of the dipole cross section are shadowed, while high transverse momentum pairs remain almost unaffected by the nucleus (color filtering). However, the actual numerical value of broadening, i.e. the increase of the square mean transverse momentum, depends on the maximum q_T included in the analysis. This is not an artifact of our approach, this is also the case in experiment.

According to (18) the numerator in (21) diverges at large q_T for the transverse cross section. Even after averaging over the projectile parton distribution, the integral is very slowly converging, and one has to introduce an upper cut-off q_T^{max} since there is a maximal transverse momentum accessible in experiment. On the other hand, the large q_T-tail of the differential cross section should be the same for nuclear and nucleon targets since no nuclear effects are expected at large q_T. For this reason one may think that the divergence cancels in the difference in Eq. (20) and renders the result cut-off independent. This might be true if no nuclear effects occured in the integrated DY cross section, i.e. if $\sigma_{DY}^{pA} = A\,\sigma_{DY}^{pN}$. However this is never the case. At long coherence time, $l_c \gg R_A$, shadowing diminishes the DY nuclear cross section, i.e. the denominator in the first term in Eq. (20). As a result the high-q_T tail of the nuclear q_T distribution is renormalized and undercompensated by the second term in Eq. (20). This is why there is sensitivity to the upper cut-off q_T^{max} in our results, and it is even more pronounced at higher energies where shadowing increases. On the other hand, at short $l_c \to 0$, where shadowing vanishes, energy loss has a similar effect of suppressing the DY cross section on nuclei [36, 2, 3].

Note that in at least some experiments [37, 38], the transverse momentum broadening is extracted from the data by fitting the points with the functional form [39]

$$\frac{d\sigma_{DY}^{pA(N)}}{d^2q_T} = \frac{\sigma_0^{pA(N)}}{\left(1 + \frac{q_T^2}{(q_0^{pA(N)})^2}\right)^n}, \tag{22}$$

where typically $n = 6$ for both a proton and a nuclear target. This means that the QCD tail of the q_T-distribution has almost no influence on the fit, which would obviously not apply in the long coherence length limit we are considering in this paper. However, nuclear broadening resulting from initial-state interactions, which dominate in the short-coherence time limit, has a gaussian tail [15], for which eq. (22) is more suited. With the ansatz (22), the mean transverse momentum squared is given by $\langle q_T^2 \rangle = q_0^2/(n-2)$, for $n > 2$, and thus broadening becomes independent of the absolute normalization $\sigma_0^{pA(N)}$ of the DY cross section.

In fig. 12 we compare A-dependences of the broadening $\delta\langle q_T^2 \rangle$ calculated with different cut-offs, $q_T^{max} = 5$ (bottom curves) and 10 GeV (upper curves). The main observations are,

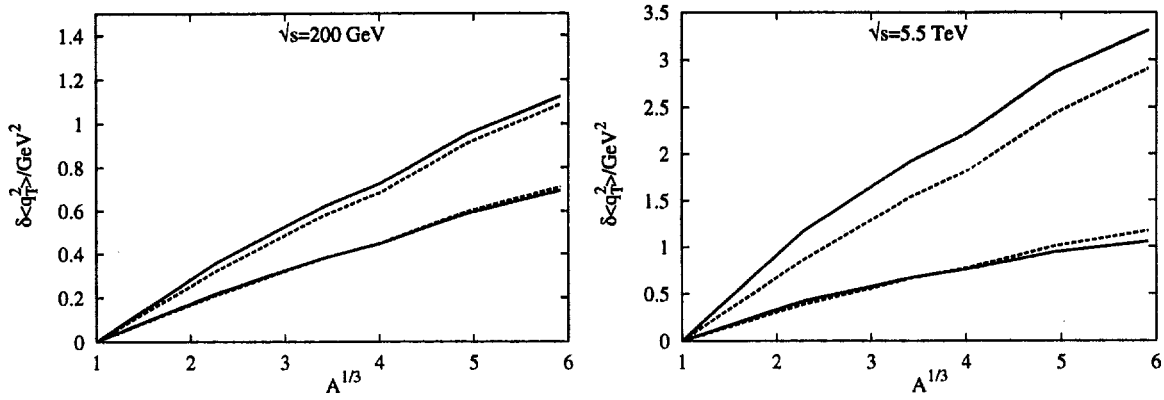

Figure 12: *Nuclear broadening for DY dileptons from pAu at RHIC and LHC. Broadening depends on the transverse momentum cutoff q_T^{max}. In each plot, the lower pair of curves is calculated for $q_T^{max} = 5$ GeV, while the upper pair is for $q_T^{max} = 10$ GeV. The solid curves include gluon shadowing, the dashed ones do not. Calculations are for the same kinematics as fig. 9.*

that broadening is roughly proportional to the length of the nuclear medium. This is true for any value of q_T^{max}. Furthermore, $\delta\langle q_T^2\rangle$ can become quite large for heavy nuclei, around 1 GeV at RHIC and around 3 GeV at LHC. While the influence of gluon shadowing on broadening is rather week, the q_T^{max}-dependence is quite strong. This is studied in more detail in fig. 13. Increasing the transverse momentum cutoff from 5 GeV to 10 GeV at RHIC energy, leads to an increase of nuclear broadening of slightly more than 50%. At LHC energy however, where one still has nuclear effecs in the transverse momentum distribution at rather large values of q_T, broadening increases by a factor of 3. Therefore, the DY process turns out to be a less than ideal tool to measure the broadening of the transverse momentum distribution for a quark propagating through nuclear matter.

Finally, we calculate the energy dependence of nuclear broadening, shown in the plot on the right in fig. 13. Again, calculations are performed for two different values of the transverse momentum cutoff. Note that the shape of the curve depends strongly on q_T^{max}. For a transverse momentum cutoff of 5 GeV, there is almost no energy dependence of $\delta\langle q_T^2\rangle$ above RHIC energy. The situation looks different if the transverse momentum cutoff is 10 GeV. In this case, broadening does increase as function of energy. It will therefore be difficult to draw conclusions from possible future data on the energy dependence of $\delta\langle q_T^2\rangle$, since presumably one will only see the cutoff dependence.

Valuable insight into the relation between shadowing and broadening is gained, if one performs the integration in the numerator of (21) analytically for $q_T^{max} \to \infty$. Without the projectile parton distribution, the result reads

$$\langle q_T^2\rangle_{A(N)} = \eta^2 + \frac{A\,C^{A(N)}(x_2)}{\sigma_{DY}^{qA(N)}(\alpha)} \int d^2\rho \left|\Psi_{\gamma^* q}^{T,L}(\rho,\alpha)\right|^2 , \tag{23}$$

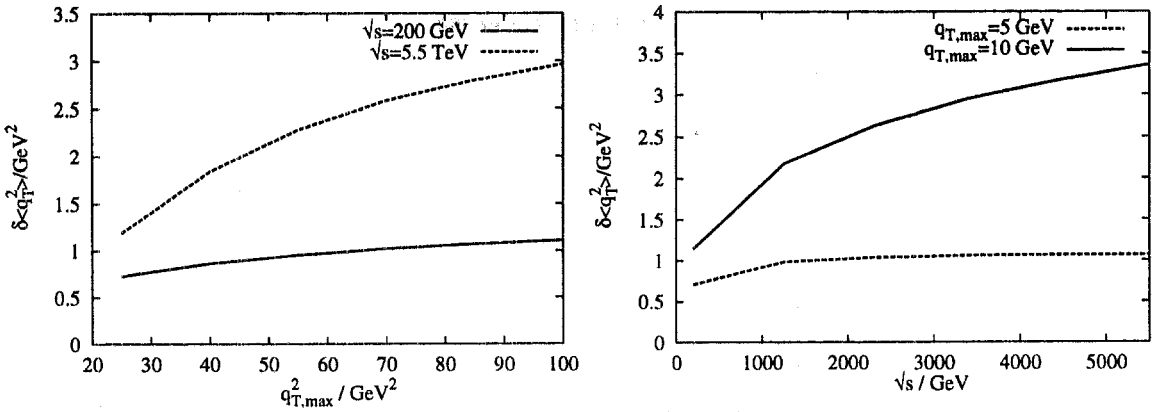

Figure 13: *The cutoff (left) and energy (right) dependence of transverse momentum broadening for pAu scattering. The calculations includes gluon shadowing. and are for the same kinematics as fig. 9.*

where the wave function squared has the form Eqs. (B.2) or (B.3); $\eta^2 = (1-\alpha)M^2 + \alpha^2 m_q^2$; $\sigma_{DY}^{qA}(\alpha) = \int d^2q_T\, \sigma_{DY}^{qA}(q_T, \alpha)$; and

$$C^{A(N)}(x_2) = \left.\frac{\partial \sigma_{q\bar{q}}^{A(N)}(\rho, x_2)}{\partial \rho^2}\right|_{\rho\to 0}. \tag{24}$$

Note that without gluon shadowing, all the difference between a nucleus and a nucleon occurs in the denominator of the second term, $\sigma_{DY}^{qA(N)}(\alpha)$. Including gluon shadowing, one has

$$C^A(x_2) = C^N(x_2) R_G(x_2). \tag{25}$$

At the same time the problem of divergence at large q_T is moved to the integral of the LC wave function squared in the second term, which has logarithmic singularity at $\rho \to 0$. Thus, the broadening Eq. (20) takes the form,

$$\delta\langle q_T^2\rangle = (\Delta R_{DY}(x_2) - \Delta R_G(x_2))\, \frac{AC^N(x_2)}{\sigma_{DY}^{qA}(\alpha)} \int d^2\rho \left|\Psi_{\gamma^* q}^{T,L}(\rho, \alpha)\right|^2, \tag{26}$$

where ΔR_{DY} and ΔR_G are nuclear suppressions for DY and for gluons, i.e. the difference from unity, cf. Eq. 8.

We arrive at the interesting conclusion that if there is no shadowing, the broadening of transverse momentum vanishes as well. This is a manifestation of a close relation between broadening and shadowing in the regime of $l_c \gg R_A$. Indeed, broadening is interpreted in the LC dipole approach as color filtering. Namely, the mean size of a $q\bar{q}$ dipole propagated through nuclear matter decreases due to absorption of large size configurations, therefore the intrinsic transverse momentum rises. Shadowing occurs due to the same phenomenon. Once one says that shadowing is negligibly small, it means that the dipole is too small to undergo multiple interactions. However, in this case no color filtering occurs either. This

rather intuitive result looks very nontrivial in the framework of parton model, where one can get broadening even without shadowing [40].

Note that gluon shadowing seems to reduce the amount of broadening in Eq. (26). This could be expected, since gluon shadowing reduces the nuclear thickness, cf. Eq. (13), and a more dilute medium leads to less broadening. However, shadowing for DY, ΔR_{DY}, increases with gluon shadowing. Numerically we find, that the influence of gluon shadowing cancels to a large amount and broadening is almost independent of R_G, see Fig. 12.

In Eq. (21) we avoided the (logarithmic) divergence in $\langle q_\perp^2 \rangle$ related to the singular behavior of $\mathrm{K}_1(x)$ at small x for transverse photons by introducing above an upper cutoff q_T^{max} on the integrals over q_T. These numerical results constitue quantitative predictions of the LC target rest frame formulation that may be compared to experiment noting that q_T^{max} is a physical parameter related to the acceptance of the spectrometer in the measurement. Motivated by the desire to understand these same numerical results analytically, we next examine the theory employing certain simplifications and approximations.

Our main approximation is to make the replacement of the fluctuation distribution by a gaussian,

$$|\Psi(\alpha,\rho)|^2 \to \frac{\alpha_{em}}{2\pi^2}((1+(1-\alpha)^2)\eta^2 n^2 e^{-k_z^2\rho^2}, \tag{27}$$

where $k_z^2 = 2\beta\eta^2$, with n^2 and β chosen to give an acceptable match to the actual fluctuation distribution, which we simplify to be

$$|\Psi(\alpha,\rho)|^2 = \frac{\alpha_{em}}{2\pi^2}((1+(1-\alpha)^2)\eta^2 K_1^2(\eta\rho), \tag{28}$$

noting that m_q is small and the longitudinal contribution is about a 10% correction to the momentum distribution. Because the distribution of fluctuations is integrable with the cutoff, the average size of the fluctuation is meaningful, and ith the gaussian wave function, the mean-square transverse spread of the fluctionation is $\langle \rho^2 \rangle = 1/k_z^2$.

With such approximations, the integral in Eq. (17) can be evaluated analytically. The result of carrying out the integrals over ρ_1, ρ_2, and q_T gives

$$\begin{aligned}\int d^2q_T\, q_T^2 \frac{d^3\sigma_{DY}^{qN}}{d(ln\alpha)\, d^2q_T} &\sim \pi \int d^2b \left\{ \frac{2\,C(\alpha)\,\alpha^2\,T_A(b)}{k_z^2} + \frac{2\,[C(\alpha)\,\alpha^2\,T_A(b)]^2}{[2\,k_z^2 + C(\alpha)\,\alpha^2\,T_A(b)]^2} \right\} \\ &\approx \pi \int d^2b \left\{ \frac{2\,C(\alpha)\,\alpha^2\,T_A(b)}{k_z^2} + \frac{[C(\alpha)\,\alpha^2\,T_A(b)]^2}{2\,k_z^4} + \ldots \right\},\end{aligned} \tag{29}$$

where we have omitted the prefactors in Eq. (27), and the expansion is useful for examining the limit of weak shadowing. Likewise,

$$\begin{aligned}\int d^2q_T \frac{d^3\sigma_{DY}^{qN}}{d(ln\alpha)\, d^2q_T} &\sim \frac{2\,\pi}{k_z^2} \int d^2b \frac{C(\alpha)\,\alpha^2\,T_A(b)}{2\,k_z^2 + C(\alpha)\,\alpha^2\,T_A(b)} \\ &\approx \pi \int d^2b \left\{ \frac{C(\alpha)\,\alpha^2\,T_A(b)}{k_z^4} - \frac{[C(\alpha)\,\alpha^2\,T_A(b)]^2}{2\,k_z^6} + \ldots \right\}.\end{aligned} \tag{30}$$

In these expressions we have introduced an effective $C = C(\alpha)$, defined independent of β so that the Drell-Yan cross section for the GW color dipole cross section is reproduced in the ρ^2 approximation to it on a nucleon,

$$C(\alpha) = \frac{\int K_1^2(\eta\rho)\sigma(\alpha\rho)d^2\rho}{n^2 \int e^{-k_z^2\rho^2}\alpha^2\rho^2 d^2\rho}. \tag{31}$$

We could optimally match approximate theory to the exact one by choosing n^2 and β numerically for a given q_T^{max}, but since our interest is insight rather than numerical precision at this point our conditons are simply the following: (1) Preserve the integral $\int \rho^2 K_1^2(\eta\rho)d^2\rho$,

$$\int_0^\infty \rho^2 K_1^2(\eta\rho)d^2\rho = n^2 \int_0^\infty \rho^2 e^{-k_z^2\rho^2} d^2\rho, \tag{32}$$

determining $n^2 = 16\beta^2/3$. (2) Adjust β to preserve $\langle\rho^2\rangle$ using the *asymptotic* form for $K_1(x)$. This gives $\beta = 1$. We determine the effective momentum cutoff corresponding to this gaussian by comparing the exact numerical value for $\langle q_T^2\rangle_N$ for the nucleon to the approximate value. The latter is obtained from the small-A limit of Eqs. (29) and (30),

$$\langle q_T^2\rangle_N = 2\langle\alpha^2(1+(1-\alpha)^2)\rangle/\langle\alpha^2(1+(1-\alpha)^2)/k_z^2\rangle, \tag{33}$$

where the brackets indicate the convolution (16) with the quark distribution function. We find that for $q_T^{max} = 10GeV$, $\langle q_T^2\rangle_N$ agrees with the RHIC values to about 10% and LHC values to about 30%.

For a nucleus, the integrals over impact parameter in in Eq. (29) and Eq. (30) may be carried out analytically for a sharp-surface density model in which the density is constant at ρ_0 out to radius $R_{1/2}$, and zero beyond. For this model, the thickness function $T_A^{(s)}(b)$ is

$$T_A^{(s)}(b) = 2\rho_0(R_{1/2}^2 - b^2)^{1/2}, \qquad b < R_{1/2} \tag{34}$$

Except for details in the surface, the shape of $T_A^{(s)}(b)$ looks very similar to that of a realistic Woods-Saxon density of half-radius $R_{1/2} = 1.1A^{1/3}$ fm, diffuseness $a = 0.545$ fm, and central density $\rho_0 = \frac{3A}{4\pi R_{1/2}^3}\frac{1}{1+\pi^2a^2/R_{1/2}^2}$. To quantify the difference, we calculated numerically the moments

$$\int d^2b T_A^n(b). \tag{35}$$

for for $1 \leq n \leq 5$ in the two cases. For nuclei $A \geq 16$, we found less than a 10% discrepency. For the sharp-surface density model $2\rho_0^2 d^2b = -\pi T_A^{(s)} dT_A^{(s)}$. Then, from Eq.(29), we find

$$\int d^2q_T\, q_T^2 \frac{d^3\sigma_{DY}^{qN}}{d(ln\alpha)\, d^2q_T} \sim \frac{4\pi^2 R_{1/2}^2}{y^2}\left[3\ln(1+y) + \frac{2}{3}y^3 + \frac{1}{2}y^2 - 2y - \frac{y}{1+y}\right]. \tag{36}$$

and from Eq. (30)

$$\int d^2q_T \frac{d^3\sigma_{DY}^{qN}}{d(ln\alpha)\, d^2q_T} \sim \frac{4\pi^2 R_{1/2}^2}{y^2k_z^2}\left[\ln(1+y) + \frac{y^2}{2} - y\right]. \tag{37}$$

where $y = C(\alpha)\alpha^2\rho_0 R_{1/2}/k_z^2$. To obtain $\langle q_T^2\rangle$ for the nucleus, it is necessary to perform a convolution of these expressions with the quark distribution function of the nucleon projectile as in Eq. (16).

It is interesting to examine the expansion of Eq.(36) and Eq. (37) in powers of y. Recalling that $k_z^2 = 1/\langle\rho^2\rangle$, and further noting that $L = 2R_{1/2}$ is the distance through the center of the nucleus, this is essentially an expansion in $y = L/2\lambda$ where $\lambda = 1/\langle\sigma_{\bar{q}q}\rangle\rho_0$ is the mean-free path of the fluctuation. For most values of α, the number of interaction mean-free paths in crossing the nucleus is tiny due to the large value of M^2 in $\eta^2 = (1-\alpha)M^2+\alpha^2 m_q^2$. However, for $\alpha \approx 1$, the mean transverse separation of the fluctuation may become relatively large (we find $\langle\rho^2\rangle^{1/2} = 0.7$ fm for $m_q = 0.2\ GeV$). In fact, for a large nucleus (A=208), we see that for RHIC energies $C(\alpha \approx 1) = 2.5$ and $y \simeq 1.5$. Clearly, these larger fluctuations have a relatively small mean-free path λ and are subject to appreciable color filtering in traversing the nucleus. For LHC, $C(\alpha \approx 1) = 5.7$ and $y \simeq 3.4$. At he same time, the amount by which $\langle q_T^2\rangle$ differs its value for a nucleon, Eq. (33), grows and hence nuclear broadening also grows. In this fashion, the physics of nuclear broadening is again seen to be directly related to color filtering for $\alpha \simeq 1$. Since the expansion of Eqs. (36) and (37) converges slowly in the region where the largest contributions to the nuclear broadening occur, it is necessary to evaluate the integrals over b and α without making an expansion to calculate $\delta\langle q_T^2\rangle$ with sufficient accuracy.

With these approximations (we have also omitted gluon shadowing, which has been shown to have a weak effect on $\delta\langle q_T^2\rangle$), we find for heavy nuclei $l_c \gg R_A$, $\delta\langle q_T^2\rangle \propto \langle T_A^2\rangle$, *i.e.* $\delta\langle q_T^2\rangle$ is very nearly linear with $A^{1/3}$, just as we found in our more exact numerical studies. The constants of proportionality are about $2.2C(x_2)$ at RHIC and $1.1C(x_2)$ at LHC, which overestimate the slope of the exact results by about 20% and 44%, respectively. Although linearity in $A^{1/3}$ would follows in the weak scattering limit, we again remark that our analytical calculations indicate substantial effects from higher-order multiple scattering.

In the opposite limit of short $l_c \to 0$, broadening is known to rise linearly with the length of the path of the quark in nuclear matter before the DY reaction occurs [41, 15],

$$\delta\langle q_T^2\rangle = C(x_2)\,\langle T_A\rangle\ , \tag{38}$$

where $\langle T_A\rangle = \int d^2b\, T_A^2(b)/A$ is the mean nuclear thickness. It is interesting to compare the nuclear dependences of broadening in the two limiting regimes $l_c \gg R_A$, Eq. (26), and $l_c \to 0$, Eq. (38). Expanding the nuclear cross section Eq. (5) in $\sigma_{q\bar{q}}^N T_A(b)$, we can then perform the integration for longitudinal DY photons (for transverse photons it diverges). Then we arrive at the same expression Eq. (38), except it acquires an extra factor

$$K = \frac{\langle[\sigma_{q\bar{q}}^N]^2\rangle}{4\left|\langle\sigma_{q\bar{q}}^N\rangle\right|^2}\ , \tag{39}$$

where

$$\langle\ldots\rangle = \int d^2\rho\,(\ldots)\left|\Psi_{\gamma^* q}^L(\rho,\alpha)\right|^2\ . \tag{40}$$

Applying the ρ^2 approximation Eq. (10) for the dipole cross we get $K = 6/5$. Thus, the broadening in the asymptotic regime $l_c \gg R_A$ matches rather well the low energy regime.

Thus, the dependence of the broadening $\delta\langle q_T^2\rangle$ on the cut-off is an unpleasant property that brings uncertainty to the comparison of theory with data. As we mentioned, it is related to the large q_T behavior Eq. (18) of the DY cross section, leading to a logarithmic divergence in the integral over q_T weighted with q_T^2,

$$\langle \sigma_{DY}^{pA}\, q_T^2\rangle \equiv \int_0^{q_T^{max}} d^2q_T\, q_T^2\, \sigma_{DY}^{pN}(q_T,\alpha)\ , \tag{41}$$

which is the numerator in (21). Since this integral has exactly the same divergence at large q_T^{max} for nuclear and nucleon targets, it must cancel in the difference,

$$\delta\langle \sigma_{DY}\, q_T^2\rangle = \langle \sigma_{DY}^{pA}\, q_T^2\rangle - A\,\langle \sigma_{DY}^{pN}\, q_T^2\rangle\ , \tag{42}$$

and the result should be independent of the upper cut-off q_T^{max} when it is sufficiently large. One can also normalize this difference dividing both terms by $A\,\langle\sigma_{DY}\rangle$. Unfortunately, the result is not an exact measure of the broadening of the transverse momentum of a quark propagating through a nucleus. However, these quantities are independent of the experimental acceptance (q_T^{max}), and this fact makes it a better observable than the broadening, Eq. (20), to compare with theory.

6 Polarization of DY pairs

In the preceding section, we separately calculated the DY cross section for transverse and longitudinal photons. In experiment, different polarizations can be distinguished by investigating the angular distribution of DY pairs. The most general form of the DY angular distribution reads [17],

$$\frac{d^4\sigma}{dx_F dM^2 d\cos\theta d\phi} \propto 1 + \lambda\cos^2\theta + \mu\sin(2\theta)\cos(\phi) + \frac{\nu}{2}\sin^2(\theta)\cos(2\phi), \tag{43}$$

where θ is the angle between the muon and the z-axis in the rest frame of the virtual photon and ϕ is the azimuthal angle. Of course, λ and ϕ depend on the choice of z-axis in the dilepton center of mass frame. Since the dipole approach is formulated in the target rest frame, it is convenient to put the z-axis in the direction of the radiated photon [9]. The target rest frame and the dilepton center of mass frame are then related by a boost in z-direction, so that the transverse polarizations are the same in the target rest frame and in the photon rest frame. Note that in the dilepton center of mass frame, the z-axis is antiparallel to the target momentum. This frame is called the u-channel frame and the curves we present are valid in this frame.

The ϕ-dependence of the cross section is difficult to measure. At RHIC, only the value of λ can be measured [37]. Since $\lambda = +1$ for transverse and $\lambda = -1$ for longitudinal, one

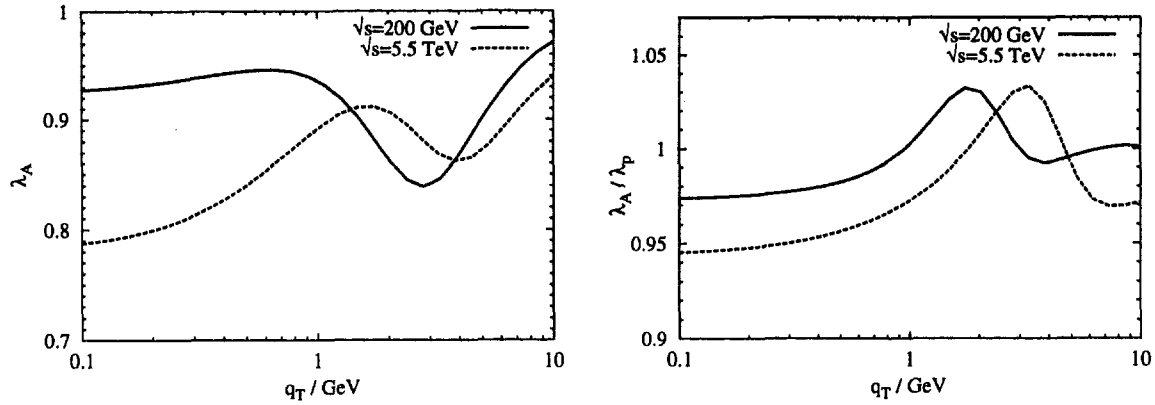

Figure 14: *The parameter λ (44) in DAu collisions at RHIC and LHC (left). The figure on the right illustrates nuclear effects on λ, by showing the ratio of λ for DAu scattering and for pp scattering. Calculations are for the same kinematics as in fig. 9.*

obtains after integration over the azimuthal angle,

$$\lambda = \frac{\sigma_T - \sigma_L}{\sigma_T + \sigma_L}. \tag{44}$$

Our results for λ at RHIC and LHC energies are shown in fig. 14. All curves are calculated including gluon shadowing. Note that at low q_T, λ shows a clear deviation from unity. This deviation increases with energy, because the longitudinal cross section is more strongly dominated by small distances than the transverse. Since the dipole cross section grows faster with energy at small separations, the relative amount of longitudinal photons at small q_T increases with energy, see fig. 9. At very large transverse momentum, λ will eventually approach unity, because the longitudinal cross section falls off steeper than the transverse one (18). It is also interesting to investigate nuclear effects on λ. For *pp* collisions, λ has been calculated previously in [11]. One sees from fig. 14, that the nucleus leads to a stronger suppression at small q_T than a proton target. This is because longitudinal photons are less shadowed at $q_T \to 0$ than transverse, fig. 10. Nuclear effects on λ vanish at very large transverse momentum, as expected.

An interesting feature of our result is that the parton model relation

$$1 - \lambda - 2\nu = 0, \tag{45}$$

which is known as Lam-Tung relation [17], is not fulfilled in the dipole approach. The violation of the Lam-Tung relation becomes apparent from the behavior of λ as $q_T \to 0$. Kinematics require that the double spin flip amplitude ν vanishes at $q_T = 0$, thus λ should approach unity. Remarkably, this relation holds to order α_s in the QCD improved parton model. Note that (45) even holds separately for the annihilation and for the Compton corrections in the parton model. Even at order α_s^2, the corrections to (45) are very small

[42], by order of magnitude $1-\lambda-2\nu \sim 10^{-2}$. Experimentally, the Lam-Tung relation is clearly violated [43], $1-\lambda-2\nu \sim -1$. However, all experimental data lie at large x_2 and are therefore not relevant for our calculation. At present, the reason for the violation of (45) is not known. Possibly, higher twist effects, included by default in our dipole approach, can provide an explanation [44]. However, it is not yet possible to apply the resummation technique [45] for logs in (q_T/M) to higher twists, which would be necessary to compare to future data on DY angular distributions from PHENIX.

The dipole formulation provides a much easier way to calculate the DY transverse momentum distribution even at low q_T. It is not surprising that the result from the $\mathcal{O}(\alpha_s)$ parton model calculation is not reproduced in our approach, because the dipole picture is not an expansion in powers of the strong coupling constant. Instead, all contributions from higher order graphs that are enhanced by a large $\log(1/x_2)$ are contained in the dipole cross section. Moreover, if we use a phenomenological parametrization of $\sigma^N_{q\bar{q}}$, some higher twists and nonperturbative effects are contained as well. The Lam-Tung relation is violated in our calculation, because of the flattening of the dipole cross section. Indeed, for a quadratically rising $\sigma^N_{q\bar{q}}(\rho,x) = C(x)\rho^2$, λ would vanish at $q_T = 0$, as can be seen from (17). Note that the remaining coefficients for the DY angular distribution (43) in the dipole formulation can be obtained from Eqs. (22)-(25) of [9]. It is easy to check that (45) is fulfilled with $\sigma^N_{q\bar{q}}(\rho,x) = C(x)\rho^2$. Finally, we would like to stress that the behavior of λ at low q_T depends heavily on the large ρ behavior of the dipole cross section, which is not well constrained by DIS and diffractive data. However, even if (7) is unrealistic at large separations, the qualitative behavior of λ will remain the same for any flattening parametrization. We therefore believe that it is worthwhile to measure λ at RHIC, because such data could give us information about the dynamics beyond the conventional parton model.

7 DY process in heavy ion collisions

As we pointed out in the Introduction it is impossible to predict nuclear shadowing for the DY process in nuclear collisions from the parton model using data for DIS and DY reaction on proton and nuclear targets. Indeed, the nuclear effects to be predicted are presented in the form,

$$R^{AB}_{DY}(x_1,x_2) \equiv \frac{\sigma^{AB}_{DY}(x_1,x_2)}{AB\,\sigma^{NN}_{DY}(x_1,x_2)}\ , \tag{46}$$

where

$$\begin{aligned}
\sigma^{AB}_{DY}(x_1,x_2) &= N\sum_f Z_f^2 \int d^2b \int d^2s\, T_A(\vec{s})T_B(\vec{b}-\vec{s})\Big[q^v_f(x_1)R^A_v(x_1,\vec{s})\,\bar{q}^s_f(x_2)R^B_s(x_2,\vec{b}-\vec{s}) \\
&+ \bar{q}^s_f(x_1)R^A_s(x_1,\vec{s})\,q^v_f(x_2)R^B_v(x_2,\vec{b}-\vec{s}) + q^s_f(x_1)R^A_s(x_1,\vec{s})\,\bar{q}^s_f(x_2)R^B_s(x_2,\vec{b}-\vec{s}) \\
&+ \bar{q}^s_f(x_1)R^A_s(x_1,\vec{s})\,q^s_f(x_2)R^B_s(x_2,\vec{b}-\vec{s})\Big]\ , \qquad (47) \\
\sigma^{NN}_{DY}(x_1,x_2) &= N\sum_f Z_f^2\Big[q^v_f(x_1)\,\bar{q}^s_f(x_2) + \bar{q}^s_f(x_1)\,q^v_f(x_2)
\end{aligned}$$

$$+ \quad + q_f^s(x_1)\,\bar{q}_f^s(x_2) + \bar{q}_f^s(x_1)\,q_f^s(x_2)\Big] \,, \tag{48}$$

where $\vec{b}$ is the impact parameter of the beam (A) and target (B) nuclei. The first two terms in Eq. (47) correspond to (i) annihilation of a valence quark of the beam with a sea antiquark of the target; (ii) a sea antiquark of the beam with a valence quark of the target. The third and fourth terms correspond to (iii) both the quark and antiquark are from the sea either of the beam or target. Provided that the Drell-Yan K-factor is independent of A, B, the overall normalization factor N in these expressions is irrelevant for shadowing Eq. (46) since it cancels in the ratio. This assumption is supported by experimental data on the K factor for various heavy ion collisions [48].

All parton distributions in Eqs. (47) – (48) are taken at the same virtuality $Q^2 = M^2$. For the sake of simplicity we assume that shadowing R_s^A is the same for sea quarks and antiquarks, and neglect the isospin noninvariance of the sea distribution at moderately small $x \sim 0.1$ [46] which can be easily taken into account.

The nuclear shadowing $R_{q_1}^A(x,\vec{s})$ is given in Sect. 7.1 below. Note that $R_q^A(x,b)$ at small x is a function of nuclear thickness. It vanishes at large impact parameters on the nuclear periphery, but reaches its maximum at $b = 0$. Data for DIS or DY reaction in pA collision provide information only about the b-integrated shadowing effect. Knowledge of only such an integrated shadowing is not sufficient for calculation of shadowing in an AB collision, Eq. (47). Nevertheless, it was assumed in [6] that shadowing is independent of impact parameter, $R_q^A(x,Q^2,b) = R_q^A(x,Q^2)$. Apparently, such an *ad hoc* assumption has no justification and leads to basic consequences which cannot be accepted. For instance, it eliminates any dependence of shadowing effects on centrality of heavy ion collision.

As we demonstrated above, the LC dipole approach provides direct access to shadowing effects dependent on impact parameter. In the following subsection, we calculate shadowing for valence and sea quarks and compare the b-integrated result to the EKS98 parameterization [4]. Of course, the impact parameter dependence of shadowing is taken into account in Sect. 7.2, where we predict shadowing for the DY reaction in a nuclear collision in the integrated form Eq. (47), as well as function of centrality. In order to calculate $R_{DY}^{AB}(x_1,x_2,b)$ for a collision with impact parameter b one should just eliminate the integration over $\vec{b}$ in the numerator of Eq. (47), and replace

$$A\,B \Rightarrow T_{AB}(b) = \int d^2s\, T_A(s)\, T_B(\vec{b}-\vec{s}) \tag{49}$$

in the denominator of Eq. (46). Comparison with the minimal-bias events for DY dilepton production in heavy ion collisions would serve as a rigorous test of the theory.

7.1 Nuclear shadowing for sea and valence quarks

Since we rely on the factorization relations Eqs. (46) – (48), we can calculate shadowing $R_s^A(x,Q^2)$ and $R_v^A(x,Q^2)$ in DIS which looks somewhat simpler, as it does not include a convolution with the initial quark distribution.

Shadowing for sea quarks is calculated with Eq. (13) and is given by

$$R_s(x,Q^2,b)=\frac{2\int_0^1 d\alpha\int d^2\rho\left|\Psi_{q\bar q}(\rho,\alpha,Q^2)\right|^2\left[1-\left(1-\frac{1}{2A}\,\sigma^N_{q\bar q}(\rho,x)R_G(x,\lambda/\rho^2,b)T_A(b)\right)^A\right]}{T_A(b)\int_0^1 d\alpha\int d^2\rho\left|\Psi_{q\bar q}(\rho,\alpha,Q^2)\right|^2\sigma^N_{q\bar q}(\rho,x)}\,. \tag{50}$$

Let us recall that this expression is valid only for the so-called "frozen" approximation, i.e. in the asymptotic regime $l_c \gg R_A$, which takes place at very small x. In the transition region $l_c \lesssim R_A$ one should employ the LC Green function technique. This was done in [47, 30], although gluon shadowing was neglected in those calculations. At very small x gluon shadowing is essential, as demonstrated above (see comparison with data from the NMC experiment in [3]).

Nuclear shadowing for valence quarks has never been calculated. This shadowing is usually believed to be small [4], if it occurs at all. We demonstrate, however, that shadowing for valence quarks is quite sizeable, even stronger than the shadowing of sea quarks. This is another new result of the present paper.

Note that we call the ratio Eq. (50) shadowing for sea quarks because the dipole cross section $\sigma^N_{q\bar q}(\rho,x)$ includes only the part that rises with energy, corresponding to gluonic exchanges in the cross-channel. Therefore, this is a part of the sea generated via gluons (there are also other sources of the sea, for instance the meson cloud of the nucleon, but they vanish linearly with x or faster). The fact that it includes only the part generated by gluons is the reason why it can be used only at very small $x < 0.01$, where the sea dominates. This part of the dipole cross section can be called the Pomeron in the language of Regge phenomenology. In the same framework, one can relate the valence quark distribution in the proton to the Reggeon part of the dipole cross section which has been neglected so far.

Thus, to include valence quarks to the dipole formulation of DIS, one should replace

$$\sigma^N_{q\bar q}(\rho,x)\Rightarrow\sigma^{\mathbb{P}}_{q\bar q}(\rho,x)+\sigma^{\mathbb{R}}_{q\bar q}(\rho,x)\,, \tag{51}$$

where the first (Pomeron) term corresponds to the gluonic part of the cross section, which we have used so far. It is responsible for the sea quark part of the nucleon structure function. The second (Reggeon) term must reproduce the distribution of valence quarks in the nucleon; this condition constraints its behavior at small x. One can guess that it has the following form,

$$\sigma^{\mathbb{R}}_{q\bar q}(\rho,x)=\tilde N\,\rho^2\sqrt{x}\,, \tag{52}$$

where $\sqrt{x}$ should reproduce the known x dependence of valence quark distribution (as, in fact, motivated by Regge phenomenology), and the factor ρ^2 is needed to respect the Bjorken scaling. The factor $\tilde N$ will cancel in what follows.

Now we are in a position to calculate shadowing for valence quarks inserting the cross section Eq. (51) into the eikonal expression Eq. (50). Clearly, only the gluonic part of the dipole cross section is subject to gluon shadowing, i.e. only the first (Pomeron) term of Eq. (51) should be multiplied by R_G. Further, if one expands the numerator in powers of

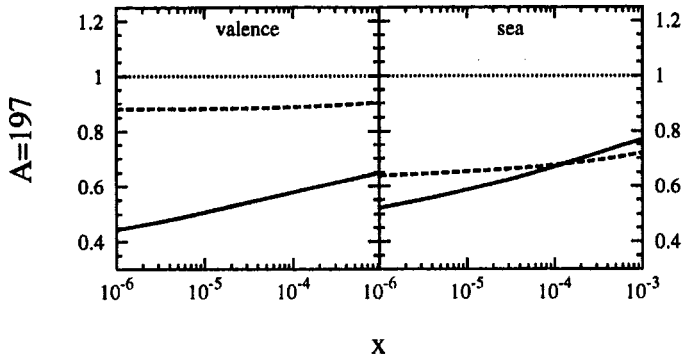

Figure 15: *Shadowing for sea and valence u-quarks in DIS off gold at $Q = 4.5$ GeV. Solid lines are calculated from Eqs. (55) - (56), while dashed curves show the EKS98 parameterization [4].*

$\sigma_{q\bar{q}}^{\mathbf{IR}}$ and picks up the linear term[4], then one arrives at the following expression for nuclear shadowing of the valence quarks,

$$R_v(x,Q^2,b) = \frac{\int_0^1 d\alpha \int d^2\rho \left|\Psi_{q\bar{q}}(\rho,\alpha,Q^2)\right|^2 \sigma_{q\bar{q}}^{\mathbf{IR}}(\rho,x) \left[1 - \frac{1}{2A}\sigma_{q\bar{q}}^{\mathbf{IP}}(\rho,x) R_G(x,\lambda/\rho^2,b) T_A(b)\right]^A}{\int_0^1 d\alpha \int d^2\rho \left|\Psi_{q\bar{q}}(\rho,\alpha,Q^2)\right|^2 \sigma_{q\bar{q}}^{\mathbf{IR}}(\rho,x)} . \tag{53}$$

This shadowing is even stronger than for sea quarks Eq. (50). Indeed, for weak shadowing we can also expand Eqs. (50) and (53) in powers of $\sigma_{q\bar{q}}^{\mathbf{IP}}$. Then one obtains a shadowing correction $1 - R_v = \frac{1}{2}\sigma_{eff} T_A$ in (53) which is twice as large as for sea quarks $1 - R_s = \frac{1}{4}\sigma_{eff} T_A$ in (50). Here $\sigma_{eff} = \langle\sigma_{q\bar{q}}^2\rangle / \langle\sigma_{q\bar{q}}\rangle$ [3].

These estimates rely, however, on the ρ^2-approximation for the dipole cross section and on the assumption that shadowing is weak. The result of our calculation, including gluon shadowing and a realistic parameterization (7) of the dipole cross section, is shown in fig. 15. We show only the b-integrated shadowing, which is given by

$$R_v(x,Q^2) = \tag{54}$$
$$\frac{\int d^2b\, T_A(b) \int_0^1 d\alpha \int d^2\rho \left|\Psi_{q\bar{q}}(\rho,\alpha,Q^2)\right|^2 \sigma_{q\bar{q}}^{\mathbf{IR}}(\rho,x) \left[1 - \frac{1}{2A}\sigma_{q\bar{q}}^{\mathbf{IP}}(\rho,x) R_G(x,\lambda/\rho^2,b) T_A(b)\right]^A}{A\int_0^1 d\alpha \int d^2\rho \left|\Psi_{q\bar{q}}(\rho,\alpha,Q^2)\right|^2 \sigma_{q\bar{q}}^{\mathbf{IR}}(\rho,x)}$$

for valence quarks and by

$$R_s(x,Q^2) = \tag{55}$$
$$\frac{2\int d^2b \int_0^1 d\alpha \int d^2\rho \left|\Psi_{q\bar{q}}(\rho,\alpha,Q^2)\right|^2 \left[1 - \left(1 - \frac{1}{2A}\sigma_{q\bar{q}}^{N}(\rho,x) R_G(x,\lambda/\rho^2,b) T_A(b)\right)^A\right]}{A\int_0^1 d\alpha \int d^2\rho \left|\Psi_{q\bar{q}}(\rho,\alpha,Q^2)\right|^2 \sigma_{q\bar{q}}^{N}(\rho,x)} .$$

[4]The small size of $\sigma_{q\bar{q}}^{\mathbf{IR}}(\rho,x)$ at small x motivates such an expansion; however, one should note that it would not be proper to include the higher powers of the Reggeon cross section. Indeed, the Reggeons correspond to planar graphs which cannot be eikonalized, since they lead to the so-called AFS (Amati-Fubini-Stangelini) planar graphs, which vanish at high energies [25].

for sea quarks. Shadowing for valence quarks is still stronger than for sea quarks, but not by a factor of 2. However, valence quark shadowing calculated in the LC approach is much stronger than in the parameterization of [4]. Unfortunately, it will be impossible to extract the low-x valence quark distribution of a nucleus from DY experiments, because the nuclear structure function is dominated by sea quarks. Maybe neutrino-nucleus scattering experiments could provide data that help to differentiate shadowing for sea and valence quarks.

7.2 Modification of the DY cross section in heavy-ion collisions

We can now make use of Eqs. (46) – (48) and predict nuclear effects for the cross section of DY lepton pair production in heavy ion collisions. We perform calculations at large x_F, where the structure function of the target nucleus, say nucleus B in (47), enters at small $x_2 \ll 0.1$ and is therefore subject to shadowing. We calculate the shadowing ratios $R_{s,v}$ in (47) as function of impact parameter from (53) – (50). However, shadowing considered in the previous section is not the only nuclear effect affecting the ratios $R_{s,v}(x_1, x_2)$. Indeed, the parton distributions of the projectile nucleus, A, are sampled at $x_1 \gtrsim 0.1$, i.e. in the region where the EMC [50] effect must be taken into account. This leads to a $10 - 20\%$ suppression at medium large x_1 and a strong enhancement at $x_1 \approx x_F \to 1$ due to Fermi motion. Also, a small $2 - 3\,\%$ enhancement is known to exist at $x_1 \sim 0.1$. All these are medium effects caused by the difference between the properties of bound and free nucleons. Since the nuclear density, apart from the surface, is approximately the same for all nuclei except for the lightest ones, one can assume that these medium effects are about the same for all bound nucleons in all nuclei. This assumption is supported by data which displays no strong A-dependence of the EMC effect from medium through heavy nuclei [50]. Of course, there is no contradiction here with our previous statement about a strong impact parameter dependence of nuclear shadowing.

For our actual calculation, we employ the EKS98 [4] parameterization of the nuclear parton distributions for nuclear effect at large x (EMC, Fermi motion). For the parton densities of a proton, which are needed as a baseline for EKS98 and for calculation of the denominator (48), we use the CTEQ5L parameterization [31]. Note that, unlike in the pA case, parton densities of the proton are not only needed at large x, but also at very small $x \ll 0.1$. The CTEQ parameterization is applicable down to $x = 10^{-5}$, which is sufficient for RHIC ($x_2 \approx 0.001$) but not for LHC, where values as low as $x \approx 10^{-6}$ are reached. For the LHC calculation, we therefore switch to GRV98LO [51], which is applicable down to $x = 10^{-9}$. All evolution codes are taken from CERNLIB PDFLIB 8.04 [32].

Our predictions for the DY modification in AA collisions at RHIC and LHC are shown in fig. 16. For comparison, we also display the analogous curves for pA scattering from 4. The plot on the left shows that DY dilepton production in $AuAu$ collisions is suppressed much stronger than in pAu collisions at the same kinematics, except for large values of x_F, where Fermi motion makes the nuclear suppression vanish. However, the strong suppression in $AuAu$ collisions is not just a combination of shadowing and the EMC effect. As one can see from the plot on the right, DY from $AuAu$ is still suppressed by about 40% compared

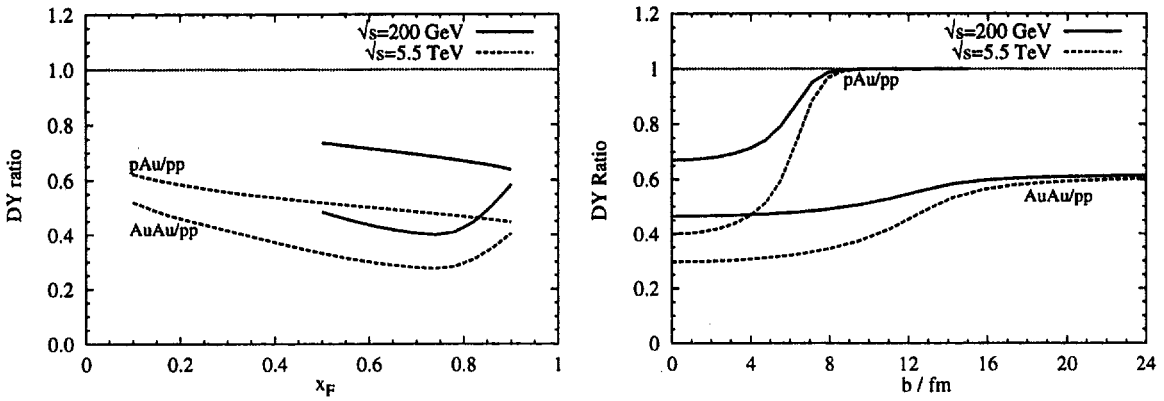

Figure 16: *Nuclear effects on the DY process in heavy ion collisions at $M = 4.5$ GeV. For comparison, the corresponding curves for pAu scattering (fig. 7) are also displayed. The plot on the right, which shows the impact parameter dependence of nuclear effects, is calculated at $x_F = 0.5$. The curves for AuAu collisions do not approach 1 at large b because of the different flavor composition of a nucleus. Note that all curves are divided by the values for pp scattering.*

to pp at very large b, where such nuclear effects are absent. Indeed, a nonnegligible part of the suppression in nucleus-nucleus collisions is due to the different flavor composition of nuclei. A heavy nucleus like gold ($A = 197$, $Z = 79$) has more neutrons than protons, thus the average nucleon in this nucleus has an excess of d-quarks over u-quarks, compared to a proton. Since d-quarks enter the lowest order expression for the DY cross section (48) with a weight factor of $Z_d^2 = 1/9$ (compared to $Z_u^2 = 4/9$) one observes an additional suppression. Finally, we mention that the suppression at large b could be even stronger than in fig. 16, because neutrons are predominantly located at large impact parameter. This effect is not taken into account in our calculation, where all nucleons are assumed to be uncorrelated.

8 Summary and outlook

We presented an analysis of nuclear effects in DY dilepton production in pA and AB collisions. All calculations are performed within the light cone dipole formalism for the DY process, because this approach suggests a very simple and intuitive treatment of nuclear effects. It essentially simplifies at high energies, where the coherence length for the DY process substantially exceeds the nuclear size. Then one can employ the eikonal formalism to describe multiple interactions, since different eigenstates of interaction do not mix. This regime, relevant to the energies of RHIC and LHC, is considered throughout the paper. Formulas for the DY cross section are sufficiently simple to incorporate realistic nuclear densities and a realistic parametrization of the dipole cross section. The predictions for RHIC and LHC presented here can therefore be compared to future data and serve as a test of the

theory.

Since we assume the coherence length to be long, gluon shadowing becomes important. The coherence length for higher Fock states is shorter than the one for the lowest Fock state, and it is usually of the order of, or shorter than, the nuclear radius. In this case, the simple eikonalization cannot be applied to gluon shadowing and we employ the LC Green function formalism, which takes account of the variations in size of the projectile fluctuations as they propagate through the nucleus. The gluon shadowing incorporated in our calculations is especially important at very high energies, or small $x_2 \ll 1$, and it makes the $q\bar{q}$-nucleus cross section saturate at a value significantly smaller than the geometrical limit of $2\pi R_A^2$.

Not surprisingly, for the total DY cross section, gluon shadowing leads to a stronger suppression than one would obtain from quark shadowing alone. Note that while fixed target experiments at medium high energies find a suppression of the DY cross section only at large Feynman-x_F, partially caused by onset of shadowing and energy loss, we expect the entire $x_F > 0$-range shadowed at RHIC and LHC. For the DY transverse momentum distribution, gluon shadowing leads to nontrivial modifications. At low lepton-pair transverse momentum, gluon shadowing enhances the suppression already expected from quark shadowing, but at intermediate transverse momentum, it strongly reduces the enhancement from the Cronin effect. This observation reminds one of the missing Cronin-enhancement in charged particle multiplicities [35]. However, the latter effect cannot be due to gluon shadowing, because the x of the data is too large.

Furthermore, we calculate nuclear broadening of the mean transverse momentum squared for DY dileptons produced in pA collisions. This quantity turns out to be divergent for radiation of transversely polarized DY photons. We demonstrate that this problem is caused by nuclear shadowing in the total DY cross section and that the two phenomena, broadening and shadowing, are closely related. As a result, the predicted broadening of the transverse momentum squared depends strongly on the upper cutoff on q_T. This is not purely a problem of the theoretical approach, as this cut-off dependence is present also in the experimental analysis. We found that $\langle \delta q_T^2 \rangle$ can vary up to a factor of three, depending on the cut-off. Moreover, a finite cut-off is always present in the experimental analysis and therefore should be taken into account in the theoretical prediction. We suggest a different observable in which the divergent tails of the q_T distribution cancel and are therefore independent of the cut-off.

We separately analyze the differential DY cross sections for transversely and longitudinally polarized pairs. In both cases, the differential cross section $d\sigma/d^2q_T$ is finite as $q_T \to 0$. This result follows naturally in the dipole approach as a consequence of the saturating dipole cross section. In the parton model, a more complicated resummation of logs in q_T/M is necessary in order to render the DY cross section finite at $q_T \to 0$. For large transverse momenta, we reproduce the behavior expected from perturbative QCD, namely $d\sigma_T/d^2q_T \propto q_T^4$ for transverse pairs and $d\sigma_L/d^2q_T \propto q_T^6$ for longitudinal.

Experimentally, the transverse and the longitudinal DY cross sections can be distinguished by investigating the angular distribution of DY pairs. We calculate the parameter λ, eq. (44), which characterizes the relative contribution of transverse and longitudinal pairs to the DY cross section as a function of the dileptons transverse momentum and, in ad-

dition, investigate nuclear effects on λ. Although these nuclear effects do not turn out to exceed 6%, the different q_T-dependence of transverse and longitudinal cross sections leads to a nonmonotonic behavior of λ that can be observed in future experiments.

Finally, we present estimates for nuclear effects in heavy ion collisions at the energies of RHIC and LHC. We make use of QCD factorization, but calculate nuclear shadowing for sea and valence quarks within the LC dipole approach. Contrary to usual expectations, we found considerable shadowing for valence quarks, stronger than for sea quarks. We calculate the nuclear suppression of DY dilepton production for $AuAu$ collisions as function of x_F and impact parameter b and find considerably stronger suppression in $AuAu$ collisions than in pAu collisions. Even at large impact parameter, the nucleus-nucleus DY cross section is reduced compared to pp as a result of flavor effects.

We leave for further study the following problems: (i) Since the approximation of a long coherence length employed for the DY process at RHIC is satisfied only at $x_F \gtrsim 0.5$, one must use the LC Green function technique in order to cover the entire range of x_F. It can also provide a proper interpretation for the Fermilab data [1]. (ii) Development of the LC dipole approach for the DY process in heavy ion collisions is still a challenge; (iii) Nuclear modification of the transverse momentum distribution and polarization effects should be also calculated for nucleus-nucleus collisions.

Acknowledgments: We are grateful to Jen-Chieh Peng for informing us about details of experiments and for useful discussions. B.Z.K. thanks the High Energy and Nuclear Theory groups at Brookhaven National Laboratory for hospitality during his visit when the present paper was completed. J.R. is grateful to Rainer Fries and Arthur Hebecker for discussion on the Lam Tung relation. This work was partially supported by the Gesellschaft für Schwerionenforschung Darmstadt (GSI), grant GSI-OR-SCH, and by the U.S. Department of Energy at Los Alamos National Laboratory under Contract No. W-7405-ENG-38.

Appendix A Calculation of gluon shadowing

Gluon shadowing is given by shadowing for longitudinal photons as

$$R_G(x,Q^2) = \frac{G_A(x,Q^2)}{AG_N(x,Q^2)} = 1 - \frac{\Delta\sigma_L^{\gamma^* A}(x,Q^2)}{A\sigma_L^{\gamma^* p}(x,Q^2)}. \tag{A.1}$$

and is calculated according to the formulas derived in [22]. In this appendix, we give some details of our calculation. Our starting point is eq. (90) of [22]:

$$\Delta\sigma_L^{\gamma^* A}(x,Q^2) = \int d^2b \int_{-\infty}^{\infty} dz_1 \int_{-\infty}^{\infty} dz_2 \Theta(z_2 - z_1)\rho_A(b,z_1)\rho_A(b,z_2)\Gamma(x,Q^2,z_2-z_1) \tag{A.2}$$

where

$$\Gamma(x,Q^2,\Delta z) \;=\; \Re \int d\ln(\alpha_G) \frac{16\alpha_{em}\left(\sum_F Z_q^2\right)\alpha_s(Q^2)C_{eff}^2}{3\pi^2 Q^2 \widetilde{b}^2}$$

$$\times \quad [(1-2\zeta-\zeta^2)\mathrm{e}^{-\zeta}+\zeta^2(3+\zeta)\mathrm{E}_1(\zeta)]$$
$$\times \quad \left[\frac{t}{w}+\frac{\sinh(\Omega\Delta z)}{t}\ln\left(1-\frac{t^2}{u^2}\right)+\frac{2t^3}{uw^2}+\frac{t\sinh(\Omega\Delta z)}{w^2}+\frac{4t^3}{w^3}\right] \quad \text{(A.3)}$$

is given by eq. (112) of [22] and

$$\Delta z = z_2 - z_1, \quad \text{(A.4)}$$
$$\Omega = \frac{\mathrm{i}B}{\alpha_G(1-\alpha_G)\nu}, \quad \text{(A.5)}$$
$$B = \sqrt{\widetilde{b}^4 - \mathrm{i}\alpha_G(1-\alpha_G)\nu C_{eff}\rho_A}, \quad \text{(A.6)}$$
$$\nu = \frac{Q^2}{2m_N x}, \quad \text{(A.7)}$$
$$\zeta = \mathrm{i}xm_N\Delta z, \quad \text{(A.8)}$$
$$t = \frac{B}{\widetilde{b}^2}, \quad \text{(A.9)}$$
$$u = t\cosh(\Omega\Delta z)+\sinh(\Omega\Delta z), \quad \text{(A.10)}$$
$$w = (1+t^2)\sinh(\Omega\Delta z)+2t\cosh(\Omega\Delta z), \quad \text{(A.11)}$$
$$\widetilde{b}^2 = (0.65\ \mathrm{GeV})^2+\alpha_G Q^2. \quad \text{(A.12)}$$

The limits for the α_G-integration are $x \le \alpha_G \le 0.1$, with α_G being the momentum fraction of the gluon relative to its parent quark. We use a running coupling constant [52]

$$\alpha_s(Q^2) = \frac{4\pi}{9\ln\left(\frac{Q^2+0.25\,\mathrm{GeV}^2}{(200\,\mathrm{MeV})^2}\right)} \quad \text{(A.13)}$$

with freezing at low scales. In (A.3), the gluon-gluon-nucleon cross section is parameterized in the form

$$\sigma^N_{GG}(\rho,\widetilde{x}) = C_{eff}(\widetilde{x})\rho^2. \quad \text{(A.14)}$$

Note that σ^N_{GG} is sampled at the energy $\widetilde{x} = x/\alpha_G$. For $\alpha_G \to x$, $\widetilde{x}$ can become greater than 0.1 and the dipole formulation is no longer valid. To overcome this problem, we employ the prescription

$$\widetilde{x} = \min(x/\alpha_G, 0.1). \quad \text{(A.15)}$$

The parameter C_{eff} is then determined from the asymptotic condition

$$\frac{\int d^2b d^2\rho\,|\Psi_{qG}(\rho)|^2\left(1-\exp\left(-\frac{1}{2}C_{eff}(\widetilde{x})\rho^2\,T_A(b)\right)\right)}{\int d^2\rho\,|\Psi_{qG}(\rho)|^2\,C_{eff}(\widetilde{x})\rho^2}$$
$$= \frac{\int d^2b d^2\rho\,|\Psi_{qG}(\rho)|^2\left(1-\exp\left(-\frac{9}{8}\sigma^N_{q\bar{q}}(\rho,\widetilde{x})\,T_A(b)\right)\right)}{\int d^2\rho\,|\Psi_{qG}(\rho)|^2\,\frac{9}{4}\sigma^N_{q\bar{q}}(\rho,\widetilde{x})}, \quad \text{(A.16)}$$

where $\sigma^N_{q\bar{q}}(\rho,\widetilde{x})$ is the dipole cross section in the saturation model of [14]. The LC wave function for radiation of a quark from a gluon, including the nonperturbative interaction

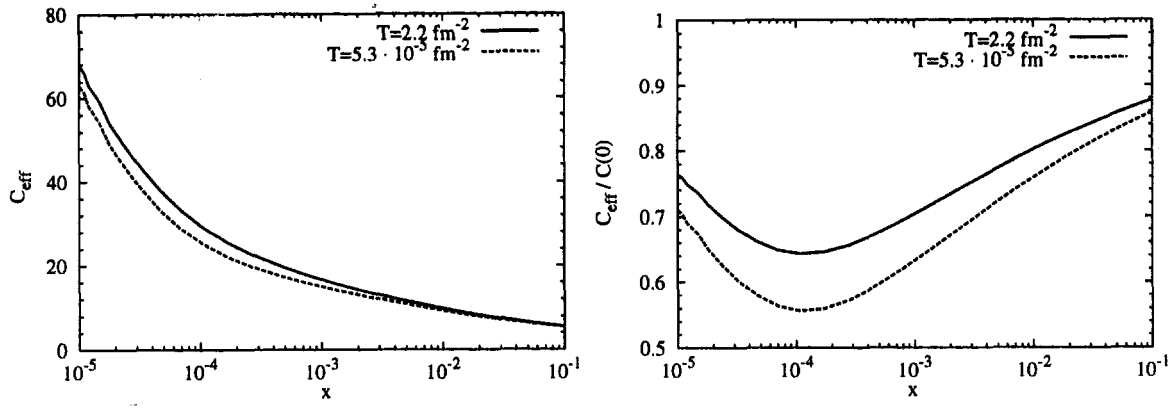

Figure 17: *The x-dependence of C_{eff} for gold at $Q^2 = 20\ GeV^2$. It is also shown, how much C_{eff} is suppressed compared to $C(\rho = 0)$. The two curves in each plot correspond to impact parameter $b = 0$ (solid) and very large impact parameter (dashed), respectively*

introduced in [22], reads

$$|\Psi_{qG}(\rho)|^2 = \frac{4\alpha_s}{3\pi^2} \frac{\exp\left(-\widetilde{b}^2\rho^2\right)}{\rho^2}. \tag{A.17}$$

The choice of C_{eff} differs from the one made in [22], where $C(\rho = 0) = d\sigma^N_{GG}(\rho)/d\rho^2|_{\rho=0}$ was employed as effective C. The prescription (A.16) is more realistic, because the C_{eff} is determined by those values of ρ which are most important for shadowing. Since the dipole cross section levels off at large separations, C_{eff} will be lower than $C(\rho = 0)$. This is illustrated in fig. 17. The $\sigma_L^{\gamma^* p}$ in the denominator of (A.2) is calculated with $C_{eff}(x)$ (instead of $\widetilde{x}$).

With a constant nuclear density ρ_A, one can integrate (A.2) twice by parts,

$$\Delta\sigma_L^{\gamma^* A}(x, Q^2) = \frac{\pi}{12}\rho_A^2 \int_0^{2R_A} dL \left(L^3 - 12R_A^2 L + 16R_A^3\right) \Gamma(x, Q^2, L), \tag{A.18}$$

with $L = 2\sqrt{R_A^2 - b^2}$.

The $q\bar{q}$-nucleus cross section in the long coherence time limit is calculated from the formula

$$\sigma^A_{q\bar{q}}(\rho, x) = 2 \int d^2b \left\{ 1 - \left(1 - \frac{\sigma^N_{q\bar{q}}(\rho, x) T_A(b) R_G(x, Q^2, b)}{2A} \right)^A \right\}, \tag{A.19}$$

where gluon shadowing as function of impact parameter b is given by

$$R_G(x, Q^2, b) = 1 - \frac{\Delta\sigma_L^{\gamma^* A}(x, Q^2, b)}{T_A(b)\sigma_L^{\gamma^* p}(x, Q^2)}, \tag{A.20}$$

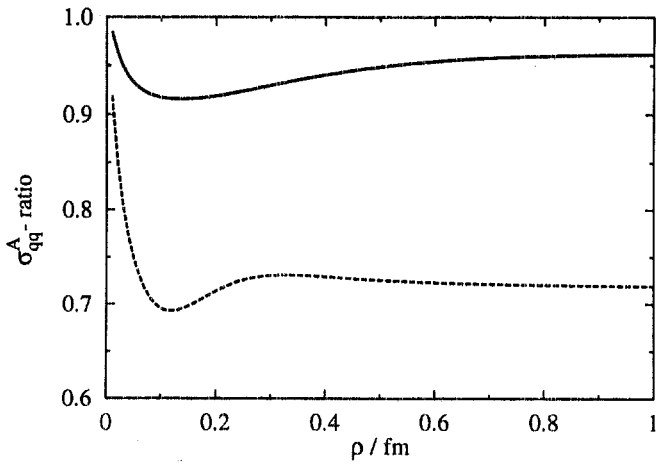

Figure 18: *This figure illustrates the influence of gluon shadowing on the $q\bar{q}$-nucleus cross section. It shows the $q\bar{q}$-nucleus cross section for gold calculated with gluon shadowing, eq. (A.19) divided by the corresponding quantity without gluon shadowing, i.e. $R_G \to 1$. The solid curve is for $x = 10^{-3}$ (RHIC), while the dashed curve is for $x = 10^{-6}$ (LHC).*

and

$$\Delta\sigma_L^{\gamma^* A}(x, Q^2, b) = \rho_A^2 \int_0^L dz\,(L - z)\,\Gamma(x, Q^2, z), \tag{A.21}$$

Furthermore, in (A.19) R_G is evaluated at the scale

$$Q^2 = \frac{1}{\rho^2} + 4\,\mathrm{GeV}^2. \tag{A.22}$$

Appendix B Calculation of the DY transverse momentum distribution

The differential DY cross section is expressed as a four-fold Fourier integral (17)

$$\begin{aligned}\frac{d\sigma(qp \to \gamma^* X)}{d\ln\alpha d^2q_T} &= \frac{1}{(2\pi)^2}\int d^2\rho_1 d^2\rho_2\, \exp[\mathrm{i}\vec{q_T}\cdot(\vec{\rho}_1 - \vec{\rho}_2)]\Psi^*_{\gamma^* q}(\alpha, \vec{\rho}_1)\Psi_{\gamma^* q}(\alpha, \vec{\rho}_2) \\ &\times \frac{1}{2}\left\{\sigma^N_{q\bar{q}}(\alpha\rho_1) + \sigma^N_{q\bar{q}}(\alpha\rho_2) - \sigma^N_{q\bar{q}}(\alpha(\vec{\rho}_1 - \vec{\rho}_2))\right\},\end{aligned} \tag{B.1}$$

where

$$\begin{aligned}\Psi^{*T}_{\gamma^* q}(\alpha, \vec{\rho}_1)\Psi^T_{\gamma^* q}(\alpha, \vec{\rho}_2) &= \frac{\alpha_{em}}{2\pi^2}\Big\{m_f^2\alpha^4 \mathrm{K}_0(\eta\rho_1)\,\mathrm{K}_0(\eta\rho_2) \\ &+ \left[1 + (1-\alpha)^2\right]\eta^2\frac{\vec{\rho}_1\cdot\vec{\rho}_2}{\rho_1\rho_2}\mathrm{K}_1(\eta\rho_1)\,\mathrm{K}_1(\eta\rho_2)\Big\},\end{aligned} \tag{B.2}$$

$$\Psi^{*L}_{\gamma^* q}(\alpha, \vec{\rho}_1)\Psi^L_{\gamma^* q}(\alpha, \vec{\rho}_2) = \frac{\alpha_{em}}{\pi^2}M^2(1-\alpha)^2\,\mathrm{K}_0(\eta\rho_1)\,\mathrm{K}_0(\eta\rho_2)\ . \tag{B.3}$$

and $\eta^2 = (1-\alpha)M^2 + \alpha^2 m_q^2$.

The Fourier-integral is inconvenient for numerical calculations, but one can perform three of the integrations analytically for arbitrary $\sigma^N_{q\bar{q}}(\alpha\rho)$.

Consider the K_0-part first. With help of the relation

$$K_0(\eta\rho) = \frac{1}{2\pi}\int d^2l \frac{e^{i\vec{l}\cdot\vec{\rho}}}{l^2+\eta^2}, \tag{B.4}$$

one finds

$$\begin{aligned}\left.\frac{d\sigma(qp\to\gamma^* X)}{d\ln\alpha d^2q_T}\right|_{K_0-\text{part}} &= \frac{\alpha_{em}}{2\pi^2}\left[m_f^2\alpha^4 + 2M^2(1-\alpha)^2\right]\frac{1}{(2\pi)^2}\int d^2\rho_1 d^2\rho_2 \frac{d^2l_1}{2\pi}\frac{d^2l_2}{2\pi} \\ &\times \frac{e^{i\vec{q}_T\cdot(\vec{\rho}_1-\vec{\rho}_2)}\, e^{-i\vec{l}_1\cdot\vec{\rho}_1}\, e^{i\vec{l}_2\cdot\vec{\rho}_2}}{(l_1^2+\eta^2)\,(l_2^2+\eta^2)} \\ &\times \frac{1}{2}\left\{\sigma^N_{q\bar{q}}(\alpha\rho_1) + \sigma^N_{q\bar{q}}(\alpha\rho_2) - \sigma^N_{q\bar{q}}(\alpha(\vec{\rho}_1-\vec{\rho}_2))\right\}. \end{aligned} \tag{B.5}$$

Note that the term in the curly brackets consists of three contributions, which depend either only on ρ_1 or on ρ_2 or on the difference $\vec{\rho}_1 - \vec{\rho}_2$. Thus, the integral (B.5) can be split into three terms. In the integral which arises from the $\sigma^N_{q\bar{q}}(\alpha\rho_1)$ part, the ρ_2-integration is trivially performed and leads to a two dimensional delta-function $\delta^{(2)}(\vec{q}_T - \vec{l}_2)$. This makes it possible to perform also the l_2 integration. The integration over l_1 gives just the MacDonald function K_0 (B.4). Thus one is left with a two fold integration over ρ_1. Provided the dipole cross section depends only on the modulus of ρ, one can use the relation

$$J_0 = \frac{1}{2\pi}\int d\phi\, e^{i\vec{l}\cdot\vec{\rho}} \tag{B.6}$$

to perform one more integration. Here, J_0 is a Bessel function of first kind. The contribution arising from $\sigma^N_{q\bar{q}}(\alpha\rho_2)$ is calculated in exactly the same way. For the $\sigma^N_{q\bar{q}}(\alpha(\vec{\rho}_1-\vec{\rho}_2))$-part one has to introduce the auxiliary variable $\vec{d} = \vec{\rho}_1 - \vec{\rho}_2$, before the procedure described above can be applied.

The K_1 part is calculated in a similar way. Note that

$$K_1(\eta\rho) = -\frac{1}{\eta}\frac{d}{d\rho}K_0(\eta\rho). \tag{B.7}$$

The K_1-part reads

$$\begin{aligned}\left.\frac{d\sigma(qp\to\gamma^* X)}{d\ln\alpha d^2q_T}\right|_{K_1-\text{part}} &= \frac{\alpha_{em}}{2\pi^2}\left[1+(1-\alpha)^2\right]\frac{1}{(2\pi)^2}\int d^2\rho_1 d^2\rho_2 \frac{d^2l_1}{2\pi}\frac{d^2l_2}{2\pi} \\ &\times \frac{e^{i\vec{q}_T\cdot(\vec{\rho}_1-\vec{\rho}_2)}\, e^{-i\vec{l}_1\cdot\vec{\rho}_1}\, e^{i\vec{l}_2\cdot\vec{\rho}_2}}{(l_1^2+\eta^2)\,(l_2^2+\eta^2)}\vec{l}_1\cdot\vec{l}_2 \\ &\times \frac{1}{2}\left\{\sigma^N_{q\bar{q}}(\alpha\rho_1) + \sigma^N_{q\bar{q}}(\alpha\rho_2) - \sigma^N_{q\bar{q}}(\alpha(\vec{\rho}_1-\vec{\rho}_2))\right\}. \end{aligned} \tag{B.8}$$

Like the K_0-part, the complete integral (B.8) is split into three pieces, corresponding to the three terms in the curly brackets. Again, one integration over ρ is immediately performed, leading to δ-functions, which allows one to do one integration over l. With the second l-integration, one recovers the MacDonald function K_1 via (B.7). For the K_1-part, one also needs the relation

$$J_1(z) = -\frac{d}{dz} J_0(z). \tag{B.9}$$

Although the calculation is slightly more cumbersome for the $\sigma^N_{q\bar{q}}(\alpha(\vec{\rho}_1 - \vec{\rho}_2))$-part, all calculations are easily performed.

Finally, one finds

$$\begin{aligned} \frac{d\sigma(qp \to \gamma^* X)}{d\ln\alpha d^2q_T} &= \frac{\alpha_{em}}{2\pi^2}\left\{\left[m_f^2\alpha^4 + 2M^2(1-\alpha)^2\right]\left[\frac{1}{{q_T}^2+\eta^2}\mathcal{I}_1 - \frac{1}{4\eta}\mathcal{I}_2\right]\right. \\ &+ \left.\left[1+(1-\alpha)^2\right]\left[\frac{\eta q_T}{{q_T}^2+\eta^2}\mathcal{I}_3 - \frac{\mathcal{I}_1}{2} + \frac{\eta}{4}\mathcal{I}_2\right]\right\}, \end{aligned} \tag{B.10}$$

with

$$\mathcal{I}_1 = \int_0^\infty dr r J_0(q_T r) K_0(\eta r) \sigma^N_{q\bar{q}}(\alpha r) \tag{B.11}$$

$$\mathcal{I}_2 = \int_0^\infty dr r^2 J_0(q_T r) K_1(\eta r) \sigma^N_{q\bar{q}}(\alpha r) \tag{B.12}$$

$$\mathcal{I}_3 = \int_0^\infty dr r J_1(q_T r) K_1(\eta r) \sigma^N_{q\bar{q}}(\alpha r). \tag{B.13}$$

The remaining integrals are evaluated numerically with the Numerical Recipes [53] routines.

References

[1] D. M. Alde *et al.*, Phys. Rev. Lett. **64**, 2479 (1990).

[2] M. B. Johnson *et al.* [FNAL E772 Collaboration], Phys. Rev. Lett. **86**, 4483 (2001) [hep-ex/0010051].

[3] M. B. Johnson *et al.*, "Energy loss versus shadowing in the Drell-Yan reaction on nuclei," hep-ph/0105195.

[4] K. J. Eskola, V. J. Kolhinen and P. V. Ruuskanen, Nucl. Phys. B **535**, 351 (1998) [hep-ph/9802350]; K. J. Eskola, V. J. Kolhinen and C. A. Salgado, Eur. Phys. J. C **9**, 61 (1999) [hep-ph/9807297].

[5] L. V. Gribov, E. M. Levin and M. G. Ryskin, Nucl. Phys. B **188**, 555 (1981); Phys. Rept. **100**, 1 (1983).

[6] K. J. Eskola, V. J. Kolhinen, P. V. Ruuskanen and R. L. Thews, hep-ph/0108093.

[7] B. Z. Kopeliovich, proc. of the workshop Hirschegg '95: Dynamical Properties of Hadrons in Nuclear Matter, Hirschegg January 16-21, 1995, ed. by H. Feldmeyer and W. Nörenberg, Darmstadt, 1995, p. 102 (hep-ph/9609385).

[8] S. D. Drell and T. Yan, Phys. Rev. Lett. **25**, 316 (1970) [Erratum-ibid. **25**, 902 (1970)].

[9] S. J. Brodsky, A. Hebecker and E. Quack, Phys. Rev. D **55**, 2584 (1997) [hep-ph/9609384].

[10] B. Z. Kopeliovich, A. Schäfer and A. V. Tarasov, Phys. Rev. C **59**, 1609 (1999), extended version in hep-ph/9808378.

[11] B. Z. Kopeliovich, J. Raufeisen and A. V. Tarasov, Phys. Lett. B **503**, 91 (2001) [hep-ph/0012035].

[12] B. Z. Kopeliovich, J. Raufeisen and A. V. Tarasov, "The color dipole approach to the Drell-Yan process in p A collisions," hep-ph/0104155.

[13] A. B. Zamolodchikov, B. Z. Kopeliovich and L. I. Lapidus, JETP Lett. **33**, 595 (1981) [Pisma Zh. Eksp. Teor. Fiz. **33**, 612 (1981)].

[14] K. Golec-Biernat and M. Wusthoff, Phys. Rev. D **59**, 014017 (1999) [hep-ph/9807513]; Phys. Rev. D **60**, 114023 (1999) [hep-ph/9903358].

[15] M. B. Johnson, B. Z. Kopeliovich and A. V. Tarasov, Phys. Rev. C **63**, 035203 (2001) [hep-ph/0006326].

[16] G. T. Bodwin, S. J. Brodsky and G. P. Lepage, Phys. Rev. D **39**, 3287 (1989).

[17] C. S. Lam and W. Tung, Phys. Rev. D **18**, 2447 (1978); Phys. Rev. D **21**, 2712 (1980).

[18] R. J. Glauber *High Energy Collision theory* in *Lectures in Theoretical Physics,* vol. 1, W. E. Brittin and L. G. Duham (eds.) Interscience, New York, 1959.

[19] A. H. Mueller, Nucl. Phys. B **335**, 115 (1990); Nucl. Phys. B **558**, 285 (1999) [hep-ph/9904404].

[20] O. V. Kancheli, Print-75-0378 (TBILISI) *In *Caneschi, L. (ed.): Regge theory of low-p(T) hadronic interactions* 312-315. (JETP Lett. 18 (1973) 274-277). (Pisma Zh. Eksp. Teor. Fiz. 18 (1973) 465-469). (see Book Index).*

[21] B. Blaettel, G. Baym, L. L. Frankfurt and M. Strikman, Phys. Rev. Lett. **70**, 896 (1993); Phys. Rev. D **55**, 98 (1997) [hep-ph/9610274].

[22] B. Z. Kopeliovich, A. Schäfer and A. V. Tarasov, Phys. Rev. D **62**, 054022 (2000) [hep-ph/9908245].

[23] A. L. Ayala, M. B. Gay Ducati and E. M. Levin, Nucl. Phys. B **493**, 305 (1997) [hep-ph/9604383].

[24] B. Kopeliovich, A. Tarasov and J. Hüfner, hep-ph/0104256, to appear in Nucl. Phys. A.

[25] V. N. Gribov, Sov. Phys. JETP **29**, 483 (1969) [Zh. Eksp. Teor. Fiz. **56**, 892 (1969)]; Sov. Phys. JETP **30**, 709 (1970) [Zh. Eksp. Teor. Fiz. **57**, 1306 (1970)].

[26] G. Bertsch, S. J. Brodsky, A. S. Goldhaber and J. F. Gunion, Phys. Rev. Lett. **47**, 297 (1981).

[27] T. Schafer and E. V. Shuryak, Rev. Mod. Phys. **70**, 323 (1998) [hep-ph/9610451].

[28] V. M. Braun, P. Górnicki, L. Mankiewicz and A. Schafer, Phys. Lett. B **302**, 291 (1993).

[29] M. D'Elia, A. Di Giacomo and E. Meggiolaro, Phys. Lett. B **408**, 315 (1997) [hep-lat/9705032].

[30] B. Z. Kopeliovich, J. Raufeisen and A. V. Tarasov, Phys. Rev. C **62**, 035204 (2000) [hep-ph/0003136].

[31] H. L. Lai *et al.* [CTEQ Collaboration], Eur. Phys. J. C **12**, 375 (2000) [hep-ph/9903282].

[32] H. Plothow-Besch, *The Parton Distribution Function Library*, Int. J. Mod. Phys. A10 (1995) 2901; *PDFLIB: Proton, Pion and Photon Parton Density Functions, Parton Density Functions of the Nucleus and α_s Calculations*, User's Manual - Version 8.04, W5051 PDFLIB, 2000.04.17, CERN-PPE.

[33] C. W. De Jager, H. De Vries and C. De Vries, Atom. Data Nucl. Data Tabl. **36**, 495 (1987).

[34] J. Raufeisen, "QCD coherence effects in high energy reactions with nuclei," hep-ph/0009358.

[35] A. Drees, nucl-ex/0105019.

[36] B.Z. Kopeliovich and F. Niedermayer, *Nuclear screening in J/Ψ and Drell-Yan pair production*, JINR-E2-84-834, Dubna 1984, a scanned version in KEK library: http://www-lib.kek.jp/cgi-bin/img_index?8504113.

[37] J.-C. Peng, private communication.

[38] P. L. McGaughey, J. M. Moss and J. C. Peng, Ann. Rev. Nucl. Part. Sci. **49**, 217 (1999) [hep-ph/9905409]; D. M. Alde *et al.*, Phys. Rev. Lett. **66**, 2285 (1991).

[39] D. M. Kaplan *et al.*, Phys. Rev. Lett. **40**, 435 (1978).

[40] L. D. McLerran and R. Venugopalan, Phys. Rev. D **49**, 2233 (1994) [hep-ph/9309289]; Phys. Rev. D **49**, 3352 (1994) [hep-ph/9311205]; Phys. Rev. D **50**, 2225 (1994) [hep-ph/9402335].

[41] J. Dolejši, J. Hüfner and B. Z. Kopeliovich, Phys. Lett. B **312**, 235 (1993) [hep-ph/9305238].

[42] E. Mirkes, Nucl. Phys. B **387**, 3 (1992); A. Brandenburg, O. Nachtmann and E. Mirkes, Z. Phys. C **60**, 697 (1993).

[43] S. Falciano *et al.* [NA10 Collaboration], Z. Phys. C **31**, 513 (1986); Phys. Rev. D **39**, 92 (1989).

[44] R. J. Fries, A. Schäfer, E. Stein and B. Müller, Nucl. Phys. B **582**, 537 (2000) [hep-ph/0002074]; R. J. Fries, B. Müller, A. Schäfer and E. Stein, Phys. Rev. Lett. **83**, 4261 (1999) [hep-ph/9907567].

[45] J. C. Collins, D. E. Soper and G. Sterman, Nucl. Phys. B **250**, 199 (1985).

[46] J. C. Peng et al. [E866/NuSea Collaboration], Phys. Rev. D **58**, 092004 (1998) [hep-ph/9804288].

[47] B. Z. Kopeliovich, J. Raufeisen and A. V. Tarasov, Phys. Lett. B **440**, 151 (1998) [hep-ph/9807211].

[48] M. C. Abreu *et al.* [NA50 Collaboration], Phys. Lett. B **410**, 337 (1997).

[49] A. B. Zamolodchikov, B. Z. Kopeliovich and L. I. Lapidus, Yad. Fiz. **35**, 129 (1982).

[50] M. Arneodo, Phys. Rept. **240**, 301 (1994).

[51] M. Gluck, E. Reya and A. Vogt, Eur. Phys. J. C **5**, 461 (1998) [hep-ph/9806404].

[52] Y. L. Dokshitzer, G. Marchesini and B. R. Webber, Nucl. Phys. B **469**, 93 (1996) [hep-ph/9512336].

[53] W. H. Press, S. A. Teukolsky, W. T. Vetterling, and B. P. Flannery, *Numerical Recipes in C*, 2nd edition, Cambridge University Press, New York, 1995.